LSND MEASUREMENTS

- DISCUSSION OF THE METHOD
- SYSTEMATIC ERRORS

The LSND Experiment

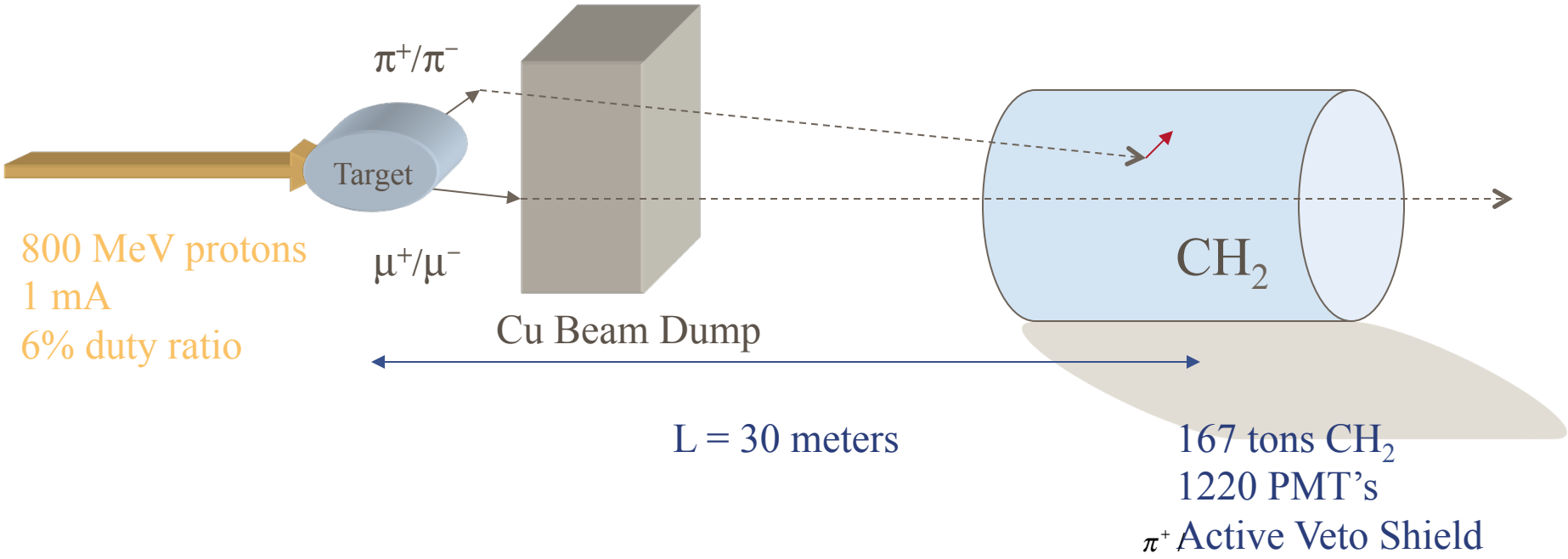

Neutrino Targets in CH_2 :

ν_μ, ν_e : neutrons in ^{12}C + electrons

ν_μ, ν_e : protons in ^{12}C + electrons + free protons

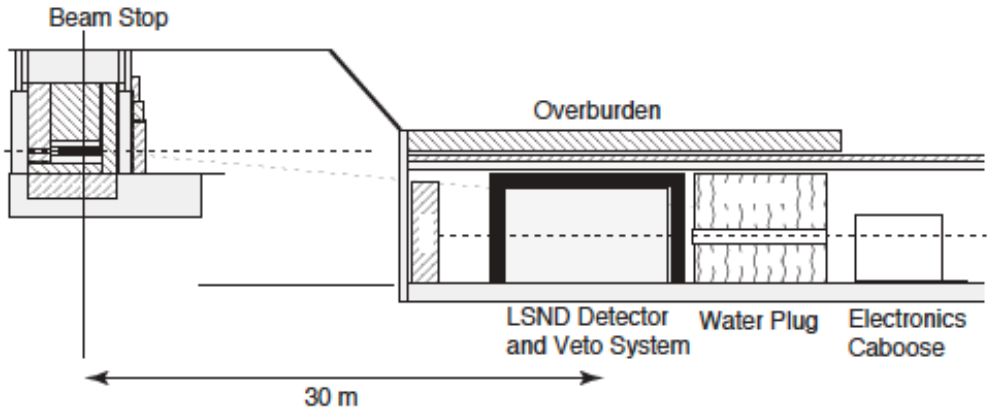

FIG. 1: The layout of the LSND detector and the A6 beam stop area.

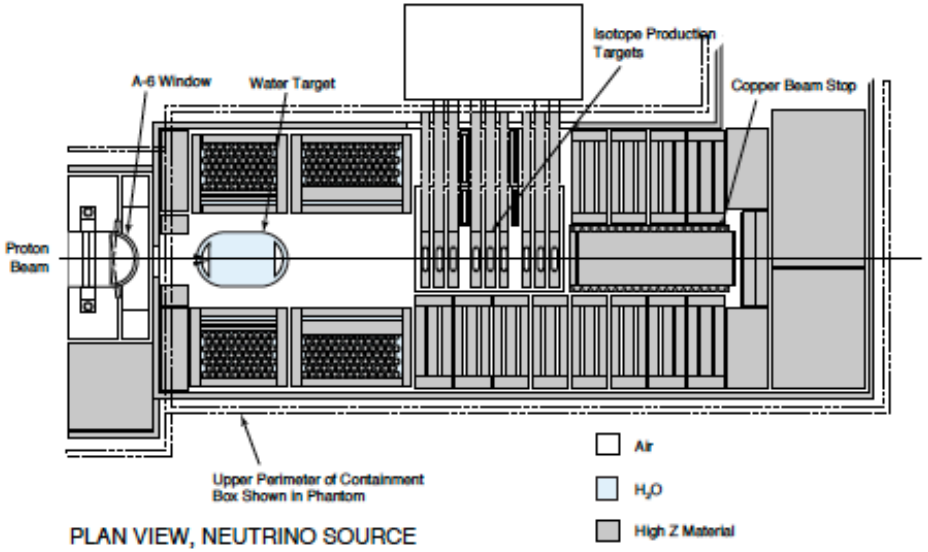

FIG. 2: The layout of the A6 beam stop, as it was configured for the 1993-1995 data taking.

TABLE I: The proton beam statistics for each of the years of running, 1993 through 1998.

Year	Charge (C)	Protons ($\times 10^{22}$)	A6 target	Active Targets
1993	1787	1.12	water	A1, A2, A6
1994	5904	3.69	water	A1, A2, A6
1995	7081	4.42	water	A1, A2, A6
1996	3789	2.37	high-Z metal	A6 & partial A2
1997	7181	4.48	high-Z metal	A6 only
1998	3154	1.97	high-Z metal	A6 only

TABLE II: The μ^- absorption rates for materials in the target area [12].

Material	Z	μ^- Absorption Rate (μs^{-1})
H	1	0.00042 ± 0.00002
Be	4	0.0074 ± 0.0005
C	6	0.0388 ± 0.0005
O	8	0.1026 ± 0.0006
Al	13	0.7054 ± 0.0013
Fe	26	4.411 ± 0.024
Cu	29	5.676 ± 0.037
Zn	30	5.834 ± 0.039
Mo	42	9.61 ± 0.15
Ta	73	12.86 ± 0.13
Pb	82	13.45 ± 0.18
U	92	12.60 ± 0.04

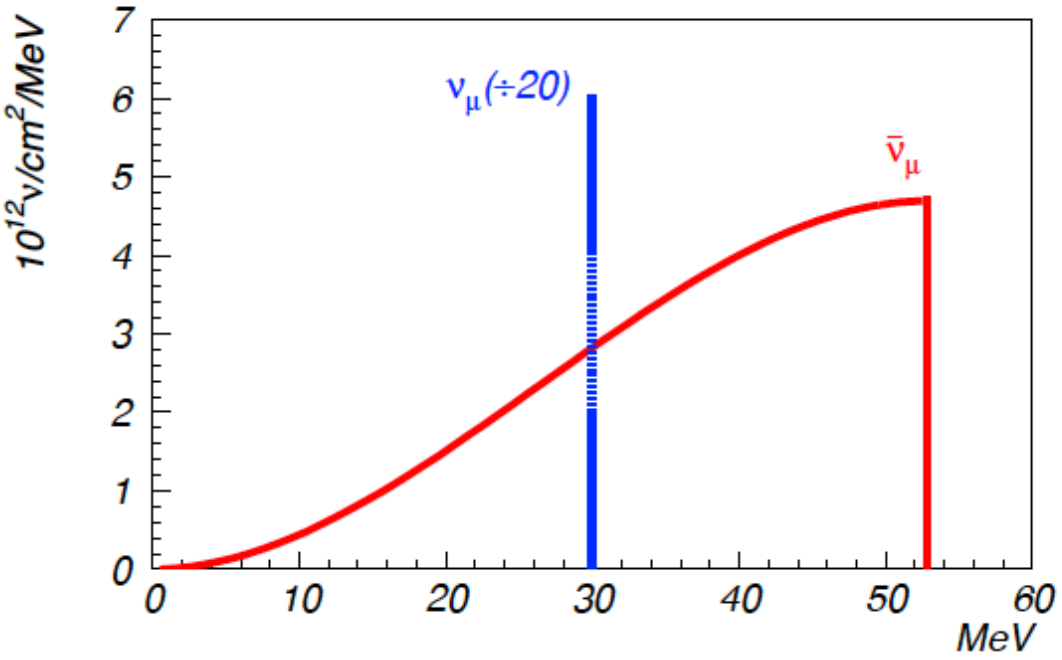
10^{12}ν/cm^2/MeV
7
6
5
4
3
2
1
0
0
10
20
30
40
50
60
MeV
ν_μ(÷20)
$\bar{\nu}_\mu$

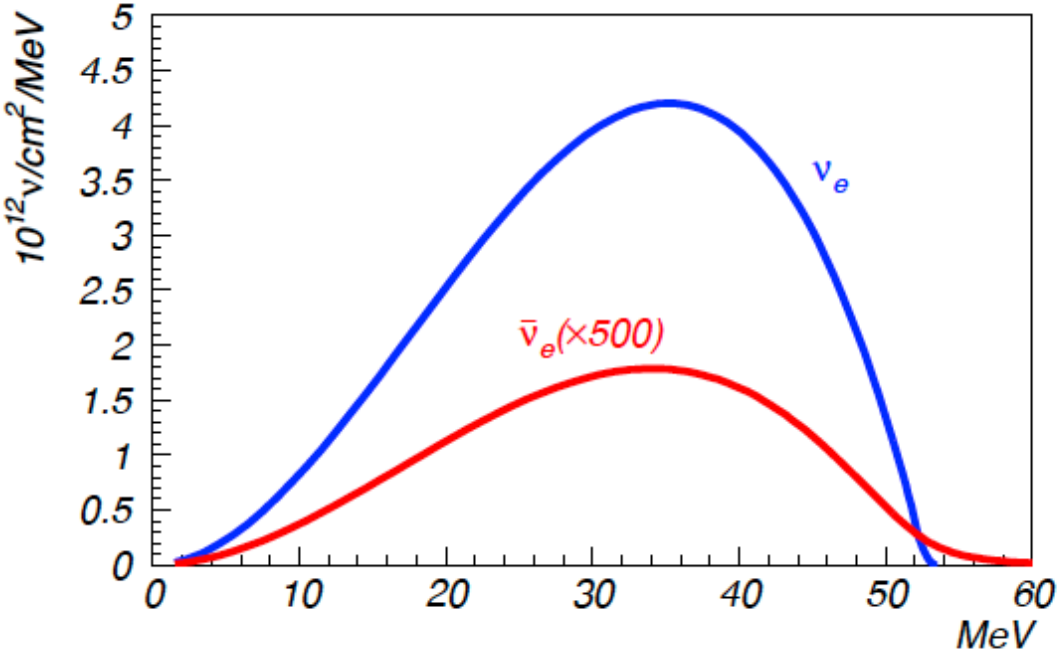
10^{12}ν/cm^2/MeV
5
4.5
4
3.5
3
2.5
2
1.5
1
0.5
0
0
10
20
30
40
50
60
MeV
ν_e
$\bar{\nu}_e$(×500)

TABLE III: Average neutrino fluxes in LSND. Both decay at rest (DAR) and decay in flight (DIF) are shown in ν/cm^2. The ν_μ and $\bar{\nu}_\mu$ DIF fluxes are above μ production threshold.

Source	Type	1993-1995 Flux	1996-1998 Flux	Total Flux
μ^+ DAR	$\bar{\nu}_\mu$ and ν_e	7.38×10^{13}	5.18×10^{13}	1.26×10^{14}
μ^- DAR	ν_μ and $\bar{\nu}_e$	5.96×10^{10}	4.87×10^{10}	1.08×10^{11}
π^+ DIF	ν_μ	1.37×10^{12}	8.26×10^{11}	2.20×10^{12}
π^- DIF	$\bar{\nu}_\mu$	1.45×10^{11}	1.11×10^{11}	2.56×10^{11}
π^+ DIF	ν_e	5.56×10^{8}	5.01×10^{8}	1.06×10^{9}
μ^+ DIF	ν_e	4.13×10^{9}	2.44×10^{9}	6.57×10^{9}

Event Time Structure

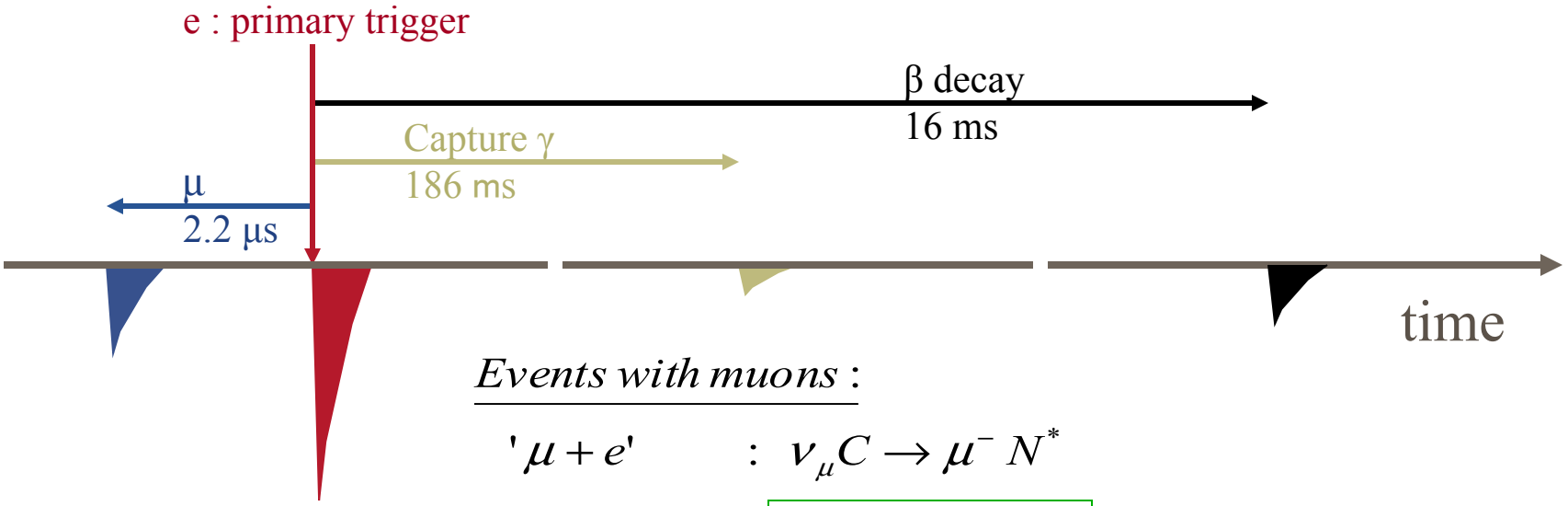

Events with muons :

$$'\mu + e' \quad : \quad \nu_\mu C \rightarrow \mu^- N^*$$

$$'\mu + e + \beta' \quad : \quad \nu_\mu C \rightarrow \mu^- N_{GS}$$

$$'\mu + e + \gamma' \quad : \quad \bar{\nu}_\mu p \rightarrow \mu^+ n$$

Events without muons :

$$'e' \quad : \quad \nu_e e \rightarrow \nu_e e, \quad \nu_e C \rightarrow e^- N^* (\nu_\mu \rightarrow \nu_e)$$

$$'e + \beta' \quad : \quad \nu_e C \rightarrow e^- N_{GS}$$

$$'e + \gamma' \quad : \quad \bar{\nu}_e p \rightarrow e^+ n \ (\bar{\nu}_\mu \rightarrow \bar{\nu}_e)$$

TABLE VI: Event categories used to determine the number of events from standard neutrino processes.

Category	Past Event	Primary Event	Future Event
e	-	ν_e	-
$e\ \beta$	-	ν_e	^{12}N decay
$e\ \gamma$	-	ν_e	n capture
$\mu\ e$	μ	e(muon decay)	-
$\mu\ e\ \beta$	μ	e(muon decay)	^{12}N decay
$e\ \gamma\ \beta$	-	ν_e	accidental γ + ^{12}N decay
$\mu\ e\ \gamma$	μ	e(muon decay)	n capture
e no β	-	ν_e	-

Event Time Structure

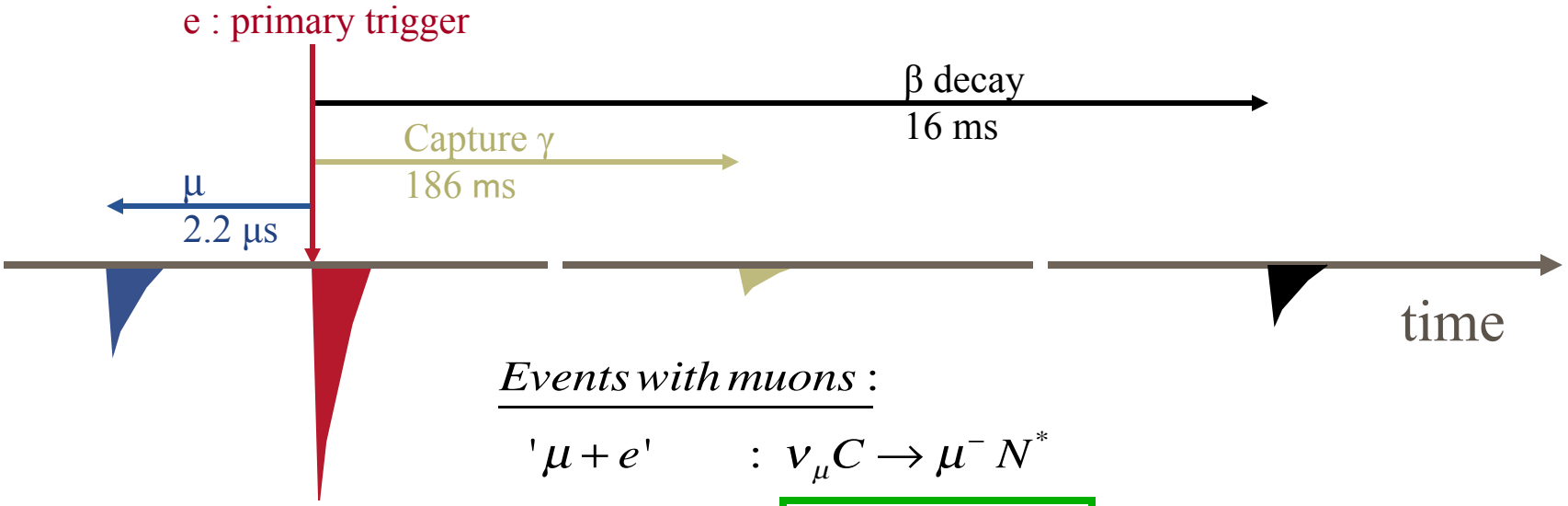

Events with muons :

$$'\mu + e' \quad : \nu_\mu C \rightarrow \mu^- N^*$$

$$'\mu + e + \beta' \quad : \nu_\mu C \rightarrow \mu^- N_{GS}$$

$$'\mu + e + \gamma' \quad : \bar{\nu}_\mu p \rightarrow \mu^+ n$$

Events without muons :

$$'e' \quad : \nu_e e \rightarrow \nu_e e,\ \nu_e C \rightarrow e^- N^* (\nu_\mu \rightarrow \nu_e)$$

$$'e + \beta' \quad : \nu_e C \rightarrow e^- N_{GS}$$

$$'e + \gamma' \quad : \bar{\nu}_e p \rightarrow e^+ n (\bar{\nu}_\mu \rightarrow \bar{\nu}_e)$$

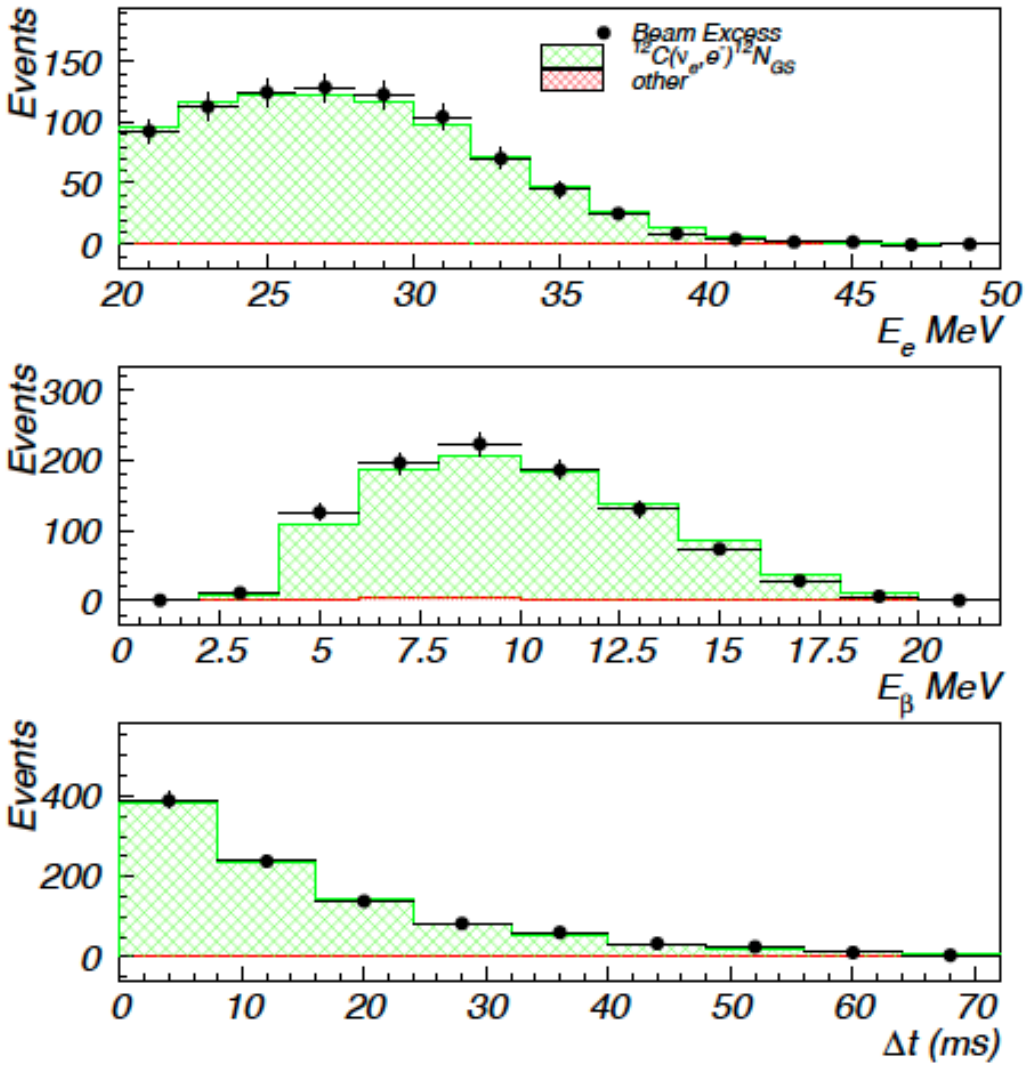

FIG. 5: The electron and β energy distributions and the time between the electron and β, Δt, for $^{12}C(\nu_e, e^-)^{12}N_{g.s.}$ scattering events.

Event Time Structure

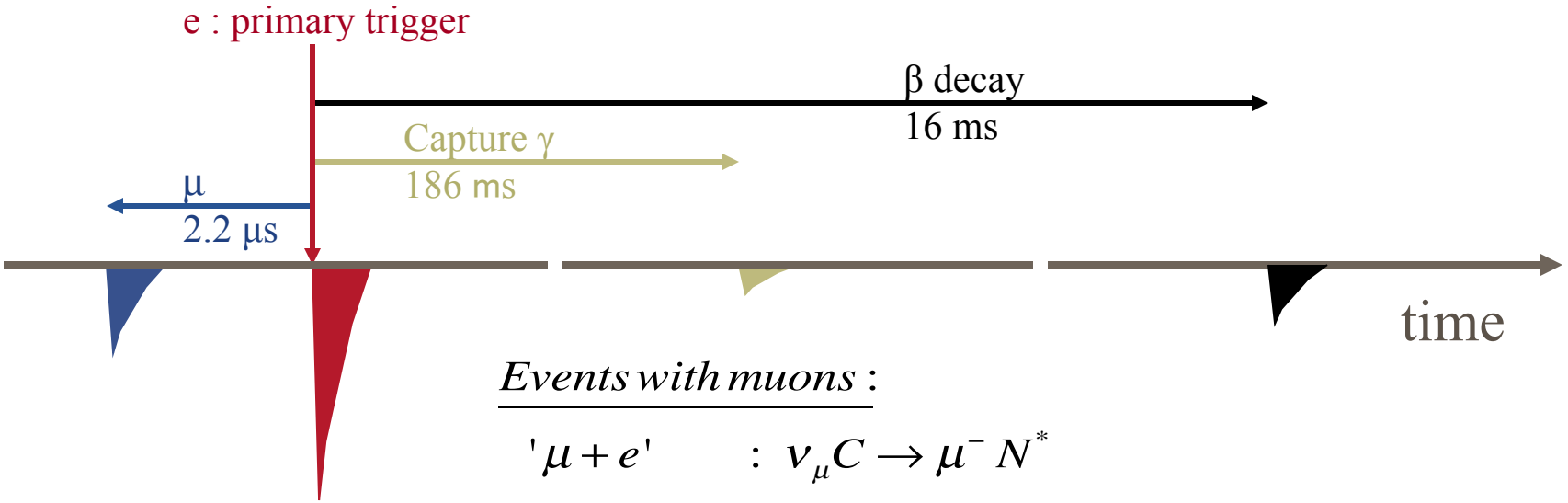

Events with muons :

$$'\mu + e' \quad : \nu_\mu C \rightarrow \mu^- N^*$$

$$'\mu + e + \beta' \quad : \nu_\mu C \rightarrow \mu^- N_{GS}$$

$$'\mu + e + \gamma' \quad : \bar{\nu}_\mu p \rightarrow \mu^+ n$$

Events without muons :

$$'e' \quad : \nu_e e \rightarrow \nu_e e,\ \nu_e C \rightarrow e^- N^* (\nu_\mu \rightarrow \nu_e)$$

$$'e + \beta' \quad : \nu_e C \rightarrow e^- N_{GS}$$

$$'e + \gamma' \quad : \bar{\nu}_e p \rightarrow e^+ n (\bar{\nu}_\mu \rightarrow \bar{\nu}_e)$$

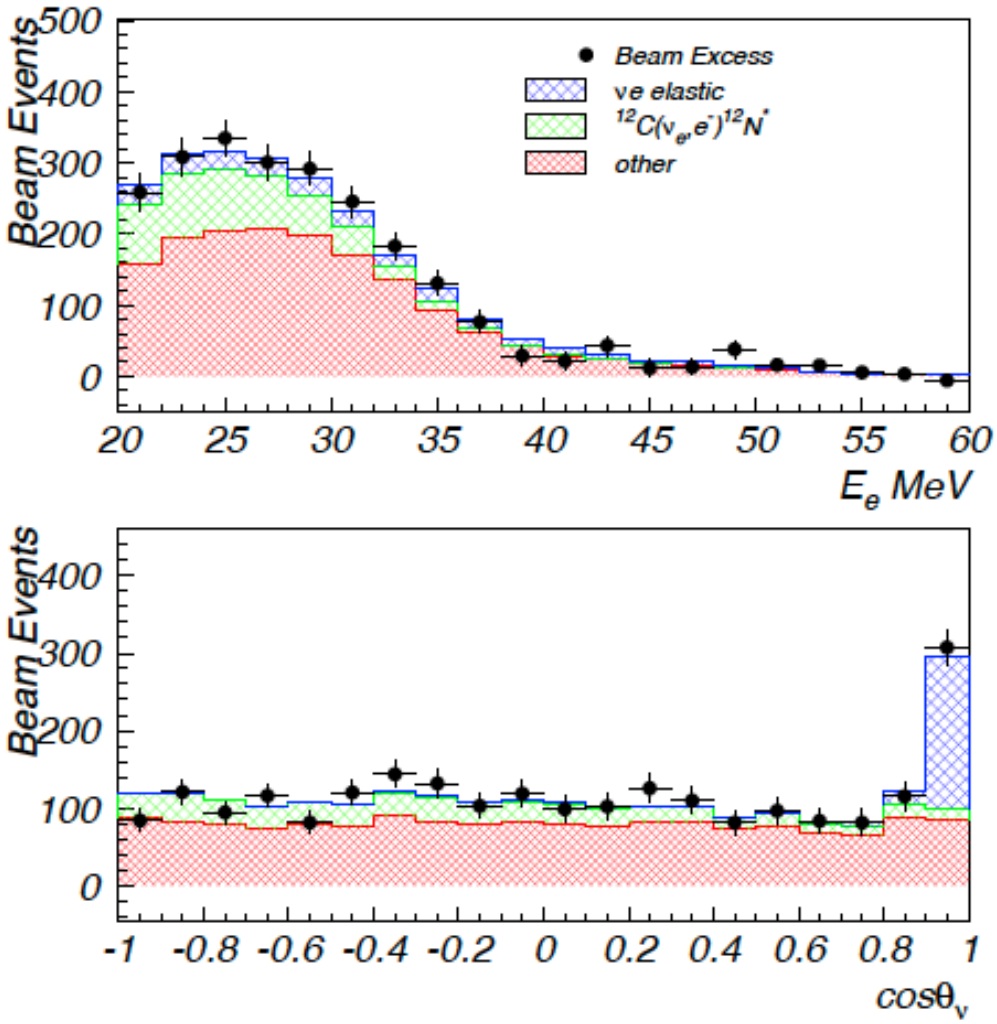

FIG. 6: The energy and angular distributions for inclusive electron events. E_e is the electron energy and θ_ν is the angle between the incident neutrino and outgoing electron directions. Neutrino-electron elastic scattering events are clearly seen near $\cos\theta_\nu \sim 1$.

Event Time Structure

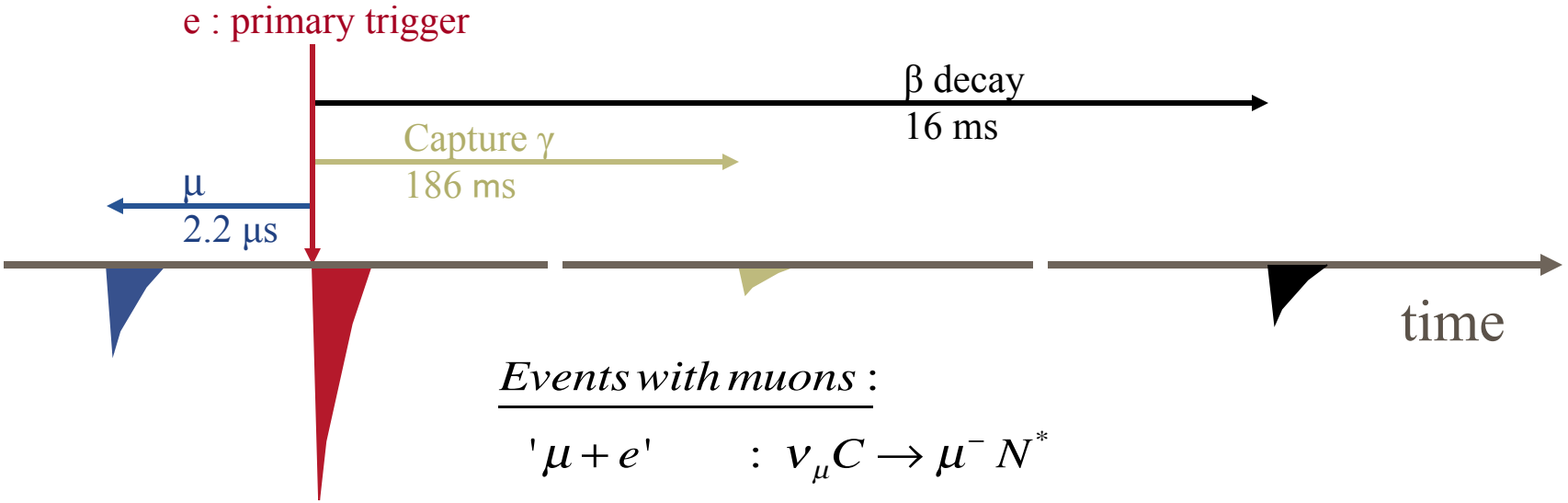

Events with muons :

$'\mu + e' \quad : \nu_\mu C \rightarrow \mu^- N^*$

$'\mu + e + \beta' \quad : \nu_\mu C \rightarrow \mu^- N_{GS}$

$'\mu + e + \gamma' \quad : \bar{\nu}_\mu p \rightarrow \mu^+ n$

Events without muons :

$'e' \quad : \nu_e e \rightarrow \nu_e e,\ \nu_e C \rightarrow e^- N^* (\nu_\mu \rightarrow \nu_e)$

$'e + \beta' \quad : \nu_e C \rightarrow e^- N_{GS}$

$'e + \gamma' \quad : \bar{\nu}_e p \rightarrow e^+ n (\bar{\nu}_\mu \rightarrow \bar{\nu}_e)$

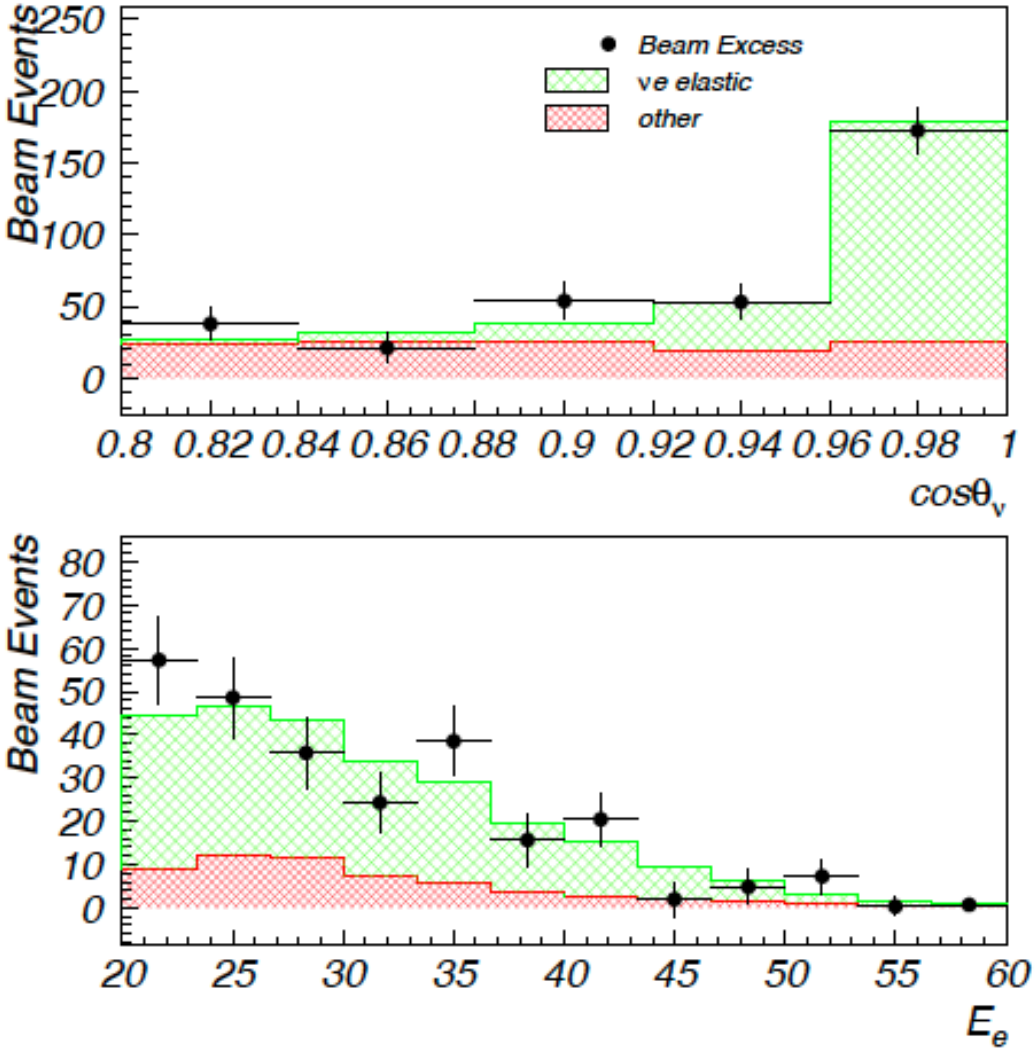

FIG. 7: The angular distribution (top plot) and the energy distribution (bottom plot) for neutrino-electron elastic scattering events with $\cos\theta_\nu > 0.9$ and with $^{12}C(\nu_e, e^-)^{12}N_{g.s.}$ events removed.

TABLE IV: Cross section uncertainties for the neutrino reactions with two-body final states that occur in LSND. The cross sections for these processes are known accurately because either related measurements can be used to constrain the matrix elements or only fundamental particles are observed. Also shown are the corresponding neutrino flux constraints.

Process	σ Constraint	σ Uncertainty	Flux Constraint
$\nu e \to \nu e$	Standard Model Process	1%	$\mu^+ \to \nu_e \bar{\nu}_\mu e^+$ DAR
$^{12}C(\nu_e, e^-)^{12}N_{g.s.}$	$^{12}N_{g.s.}$	5%	$\mu^+ \to \nu_e \bar{\nu}_\mu e^+$ DAR
$^{12}C(\nu_\mu, \mu^-)^{12}N_{g.s.}$	$^{12}N_{g.s.}$	5%	$\pi^+ \to \nu_\mu \mu^+$ DIF
$p(\bar{\nu}_\mu, \mu^+)n$	neutron decay	5%	$\pi^- \to \bar{\nu}_\mu \mu^-$ DIF

TABLE V: The average efficiencies for electrons in the fiducial volume with energies in the range $20 < E_e < 60$ MeV.

Criteria	Efficiency
Electron Reduction	
Energy > 15 MeV	1.00
Veto Hits < 4	0.98 ± 0.01
No Laser Tag	1.00
Loose Electron PID	0.96 ± 0.01
Vertex > 10 cm from PMTs	1.00
Cosmic Muon Cut	0.92 ± 0.01
Electron Selection	
$\Delta t_{past} > 12\mu$s	0.96 ± 0.01
$\Delta t_{future} > 8\mu$s	0.99 ± 0.01
No bottom veto hit	1.00
$-1.5 < \chi'_{tot} < 0.5$	0.84 ± 0.01
$0.3 < \chi^{old}_{tot} < 0.65$ (1993 only)	0.98 ± 0.01
85ns < t_{event} < 210ns	1.00
$\Delta t^{best}_{veto} > 30$ns	0.97 ± 0.01
D > 35 cm	0.88 ± 0.02
$N_\gamma < 1, E > 60$	1.00
$N_\gamma < 2, E < 60$	1.00
Deadtime	
DAQ & Tape Deadtime	0.96 ± 0.02
Veto Deadtime	0.76 ± 0.02
Total	0.42 ± 0.03

Event Time Structure

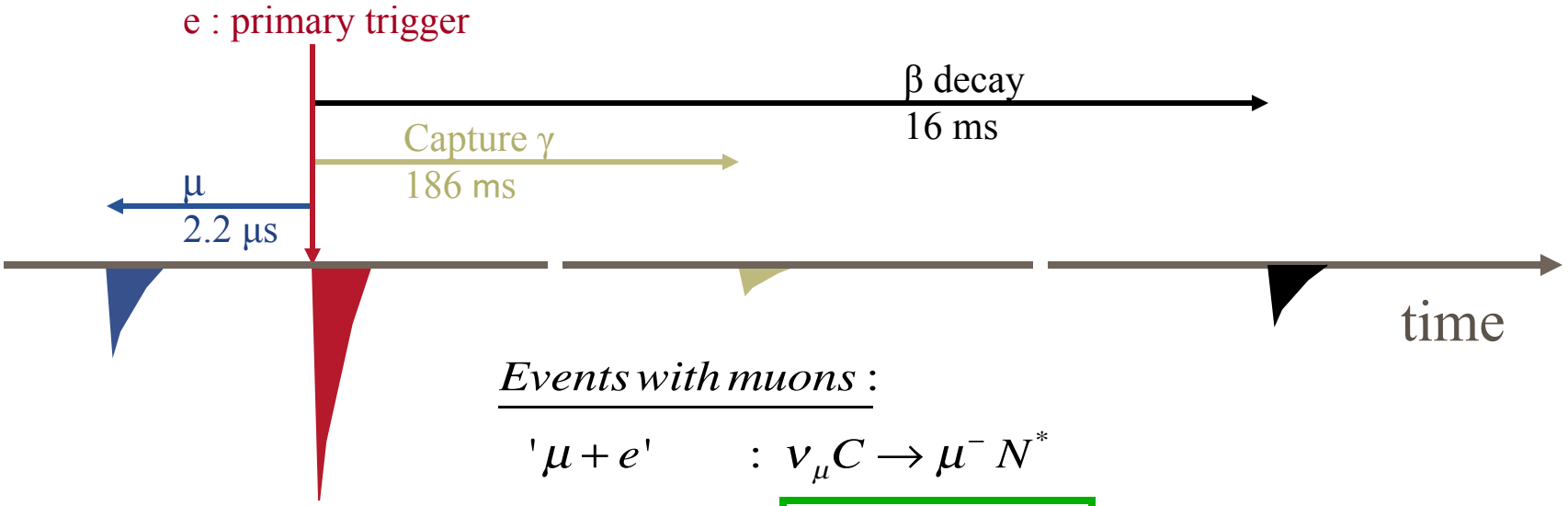

Events with muons :

$$'\mu + e' \quad : \nu_\mu C \rightarrow \mu^- N^*$$

$$'\mu + e + \beta' \quad : \nu_\mu C \rightarrow \mu^- N_{GS}$$

$$'\mu + e + \gamma' \quad : \bar{\nu}_\mu p \rightarrow \mu^+ n$$

Events without muons :

$$'e' \quad : \nu_e e \rightarrow \nu_e e,\ \nu_e C \rightarrow e^- N^* (\nu_\mu \rightarrow \nu_e)$$

$$'e + \beta' \quad : \nu_e C \rightarrow e^- N_{GS}$$

$$'e + \gamma' \quad : \bar{\nu}_e p \rightarrow e^+ n (\bar{\nu}_\mu \rightarrow \bar{\nu}_e)$$

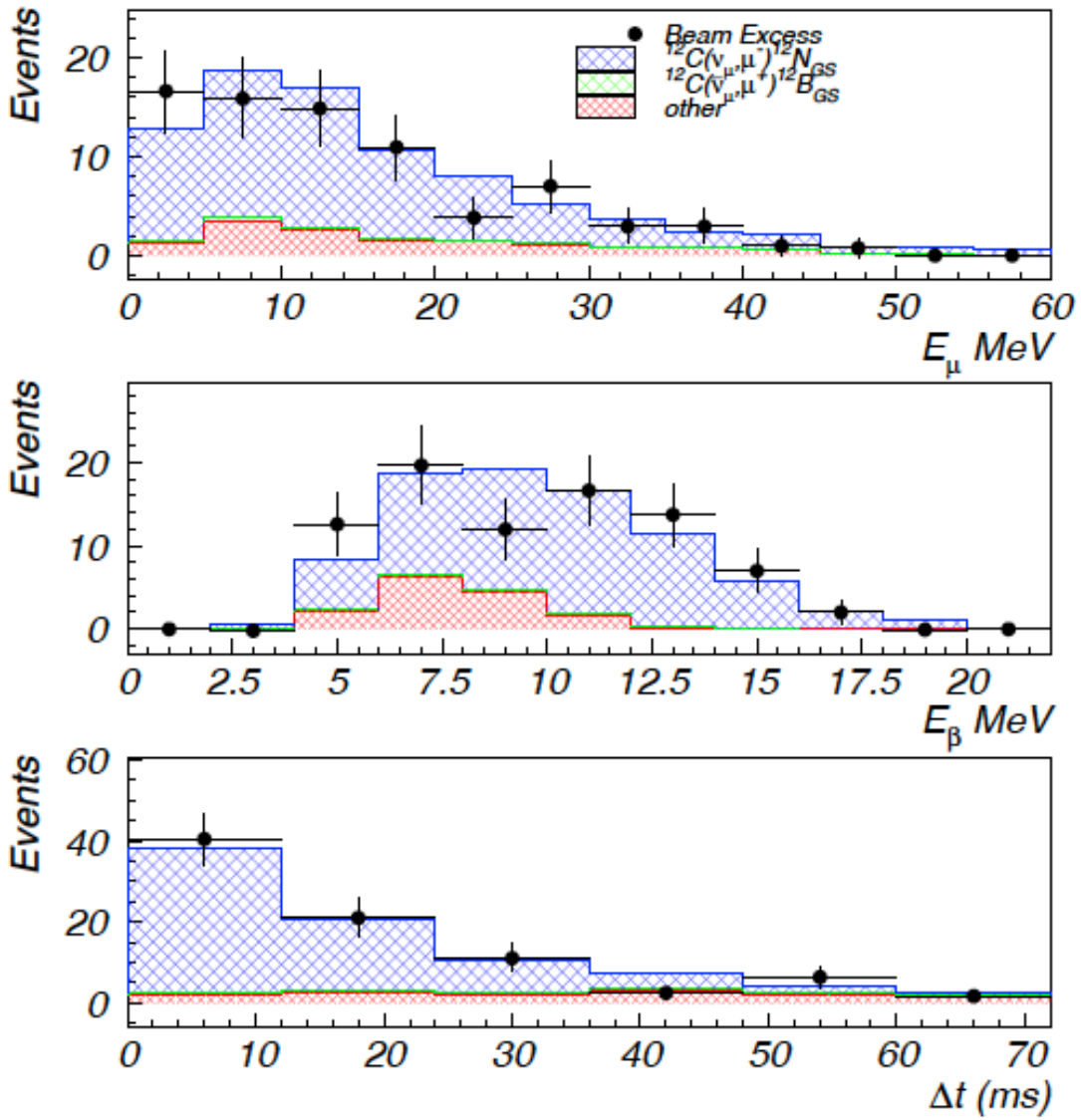

FIG. 8: The muon and β energy distributions (electron energy equivalent) and the time between the muon and β for $^{12}C(\nu_\mu,\mu^-)^{12}N_{g.s.}$ scattering events.

Event Time Structure

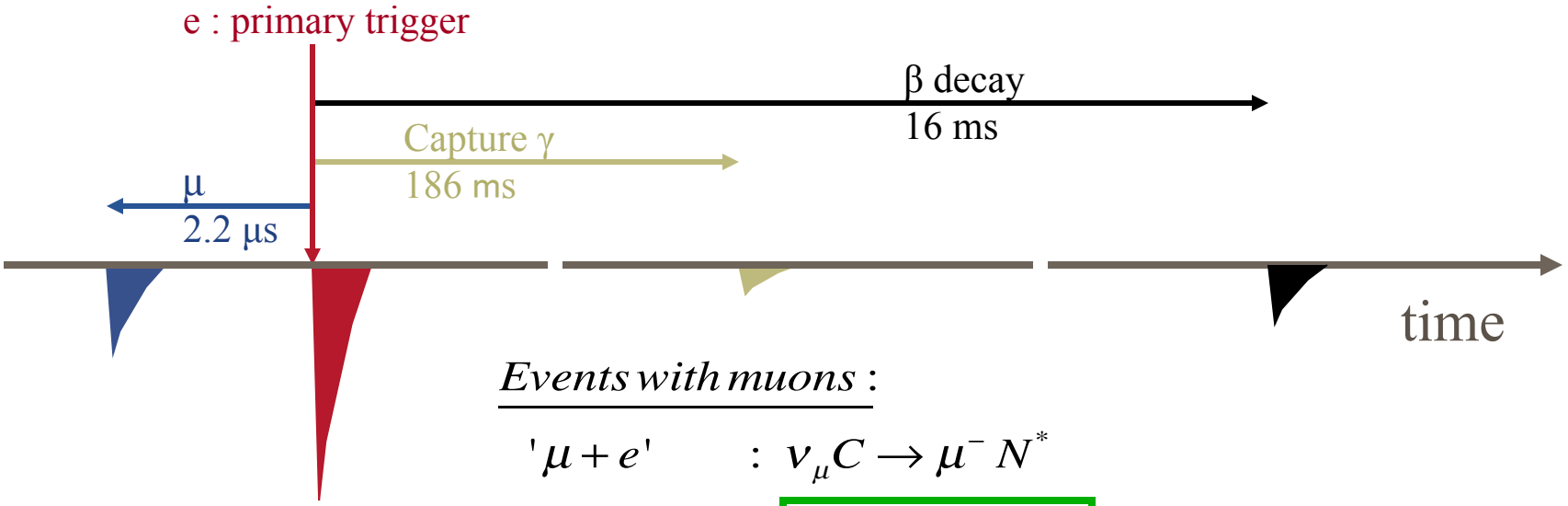

Events with muons :

$$'\mu + e' \quad : \nu_\mu C \rightarrow \mu^- N^*$$

$$'\mu + e + \beta' \quad : \nu_\mu C \rightarrow \mu^- N_{GS}$$

$$'\mu + e + \gamma' \quad : \bar{\nu}_\mu p \rightarrow \mu^+ n$$

Events without muons :

$$'e' \quad : \nu_e e \rightarrow \nu_e e,\ \nu_e C \rightarrow e^- N^* (\nu_\mu \rightarrow \nu_e)$$

$$'e + \beta' \quad : \nu_e C \rightarrow e^- N_{GS}$$

$$'e + \gamma' \quad : \bar{\nu}_e p \rightarrow e^+ n (\bar{\nu}_\mu \rightarrow \bar{\nu}_e)$$

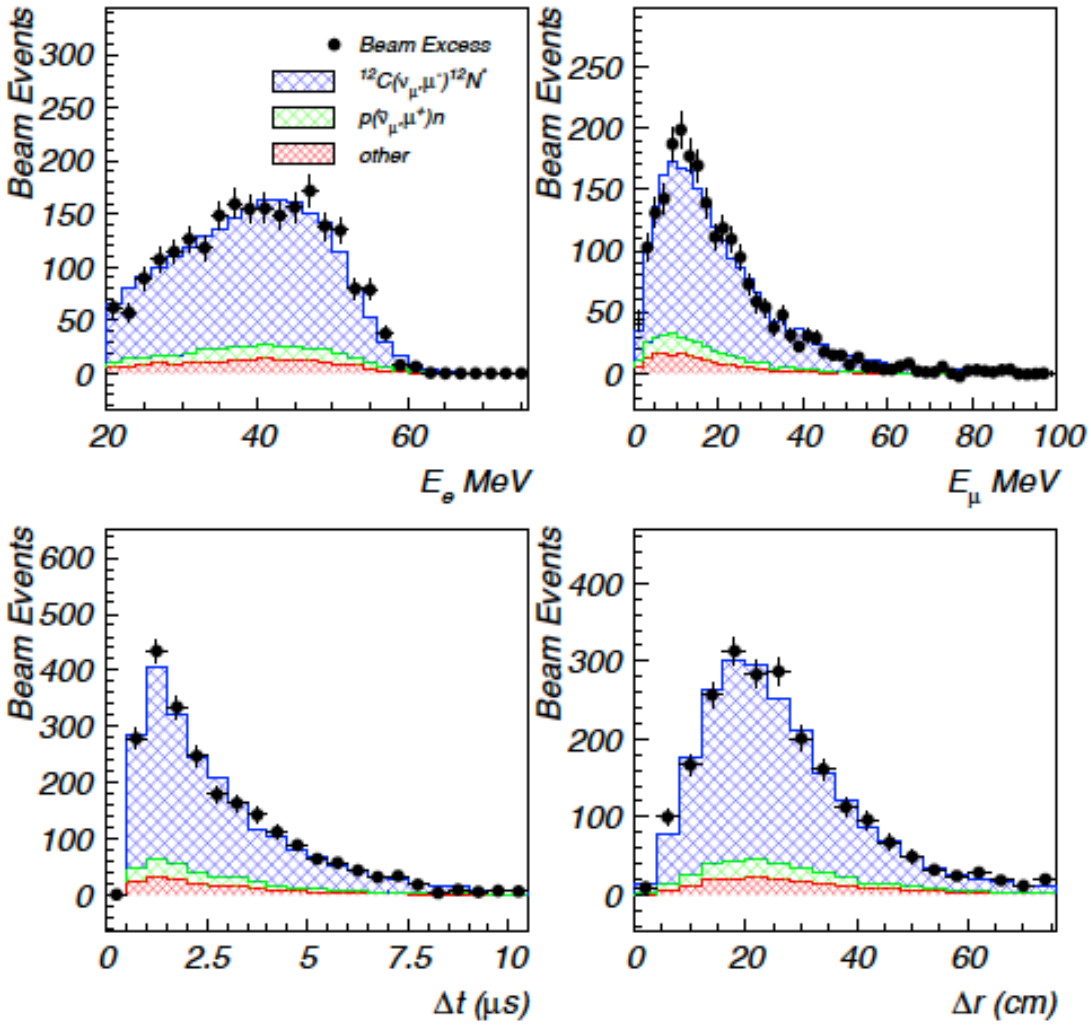

FIG. 9: The Michel electron and muon energy distributions (electron energy equivalent), the time between the muon and electron, Δt, and the distance between the reconstructed electron position and muon position, Δr, for $\nu_\mu C \to \mu^- N$, $\bar{\nu}_\mu C \to \mu^+ B$, and $\bar{\nu}_\mu p \to \mu^+ n$ inclusive scattering events.

TABLE VII: Parameters adjusted during the least squares fit procedure, along with the fitted correction values, central correction values, and nominal parameter values.

Parameter	Fitted Correction Value	Central Correction Value	Nominal Parameter Value
Flux Parameters			
Φ_{DIF}	0.88 ± 0.09	1.00 ± 0.15	$0.22 \times 10^{13} \nu/cm^2$
Φ_{DAR}	1.01 ± 0.05	1.00 ± 0.07	$12.6 \times 10^{13} \nu/cm^2$
$\frac{\pi^-}{\pi^+}$ *ratio*	0.90 ± 0.19	1.00 ± 0.10	0.12
Cross Section Parameters			
$\sigma(\nu_\mu^{12}C \rightarrow \mu^-\ ^{12}N^*)$	0.68 ± 0.23	1.00 ± 0.25	$15.2 \times 10^{-40}\ cm^2$
$\sigma(\bar{\nu}_\mu p \rightarrow \mu^+ n)$	0.97 ± 0.05	1.00 ± 0.05	$4.9 \times 10^{-40}\ cm^2$
$\sigma(\nu_e^{12}C \rightarrow e^-\ ^{12}N_{g.s.})$	1.01 ± 0.05	1.00 ± 0.05	$9.2 \times 10^{-42}\ cm^2$
$\sigma(\nu_e^{12}C \rightarrow e^-\ ^{12}N^*)$	1.02 ± 0.13	1.00 ± 0.25	$4.1 \times 10^{-42}\ cm^2$
$\sigma(\nu_e^{13}C \rightarrow e^-\ ^{13}N)$	0.93 ± 0.28	1.00 ± 0.30	$0.53 \times 10^{-40}\ cm^2$
Efficiency Parameters			
ϵ_μ	1.00 ± 0.06	1.00 ± 0.07	0.93
ϵ_β	1.00 ± 0.04	1.00 ± 0.07	0.65
ϵ_e	1.00 ± 0.05	1.00 ± 0.07	0.42
ϵ_γ	0.91 ± 0.03	1.00 ± 0.07	0.60
duty ratio	0.95 ± 0.03	1.00 ± 0.03	0.060

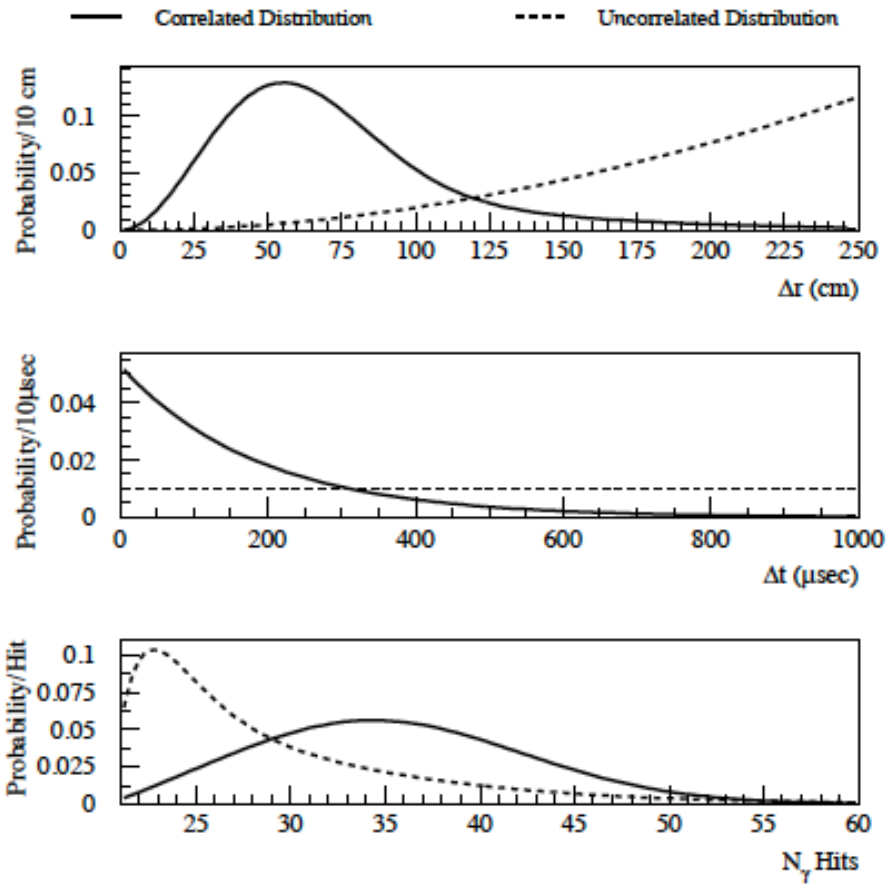

FIG. 10: Distributions for correlated 2.2 MeV γ (solid curves) and accidental γ (dashed curves). The top plot shows the distance between the reconstructed γ position and positron position, Δr, the middle plot shows the time interval between the γ and positron, Δt, and the bottom plot shows the number of hit phototubes associated with the γ, N_{hits}.

Event Time Structure

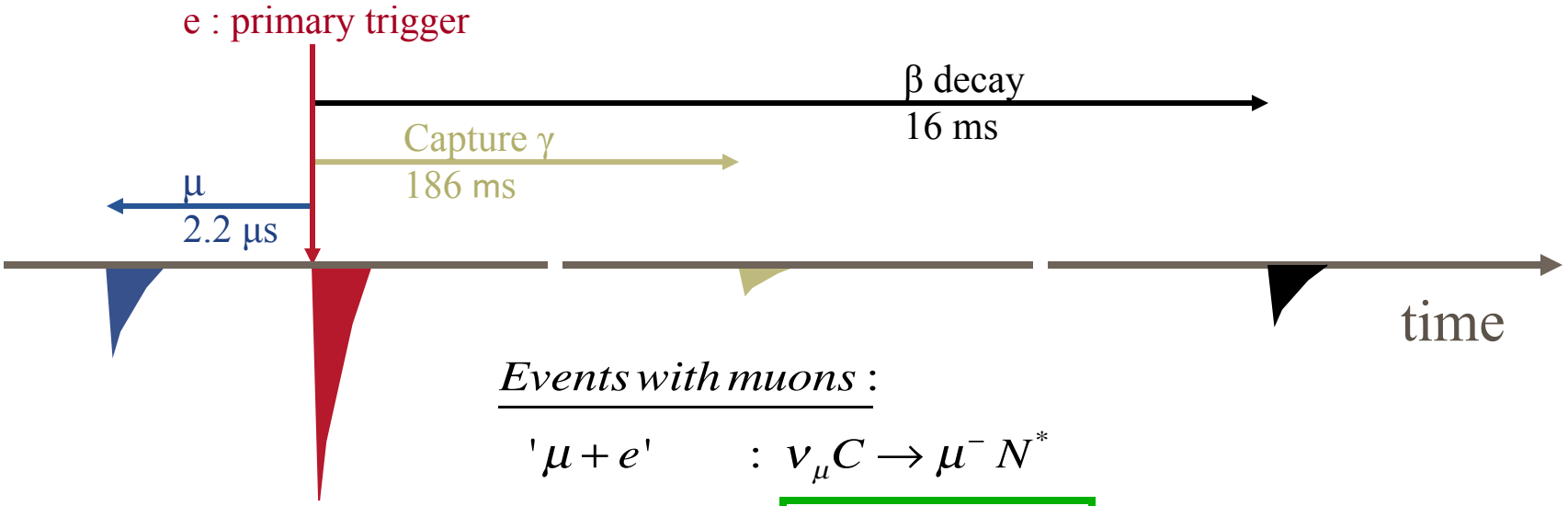

Events with muons :

$$'\mu + e' \quad : \nu_\mu C \rightarrow \mu^- N^*$$

$$'\mu + e + \beta' \quad : \nu_\mu C \rightarrow \mu^- N_{GS}$$

$$'\mu + e + \gamma' \quad : \bar{\nu}_\mu p \rightarrow \mu^+ n$$

Events without muons :

$$'e' \quad : \nu_e e \rightarrow \nu_e e,\ \nu_e C \rightarrow e^- N^* (\nu_\mu \rightarrow \nu_e)$$

$$'e + \beta' \quad : \nu_e C \rightarrow e^- N_{GS}$$

$$'e + \gamma' \quad : \bar{\nu}_e p \rightarrow e^+ n (\bar{\nu}_\mu \rightarrow \bar{\nu}_e)$$

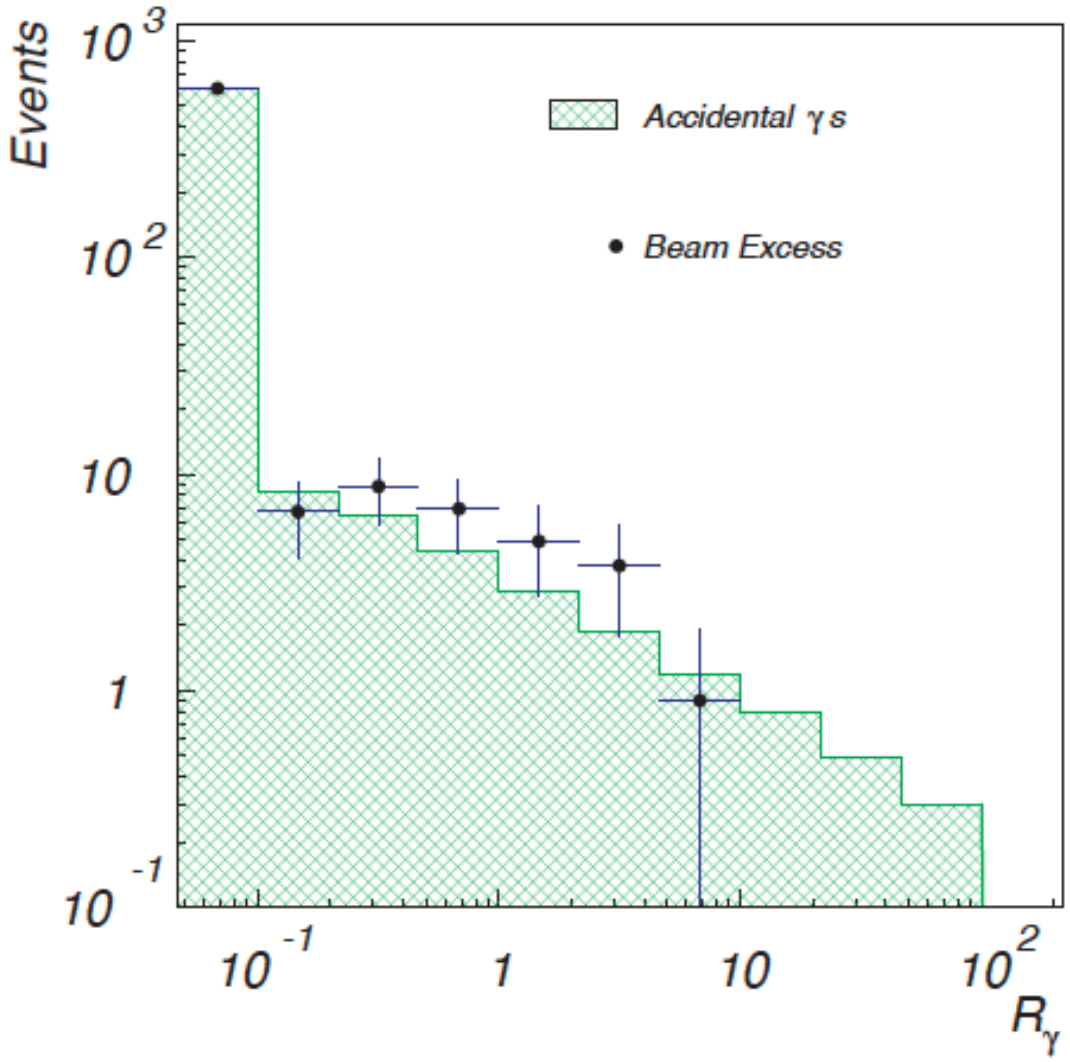

FIG. 11: The R_γ distribution for $\nu_e C \to e^- N_{g.s.}$ exclusive events, where the $N_{g.s.}$ β decays. The distribution is consistent with a pure accidental γ shape.

Event Time Structure

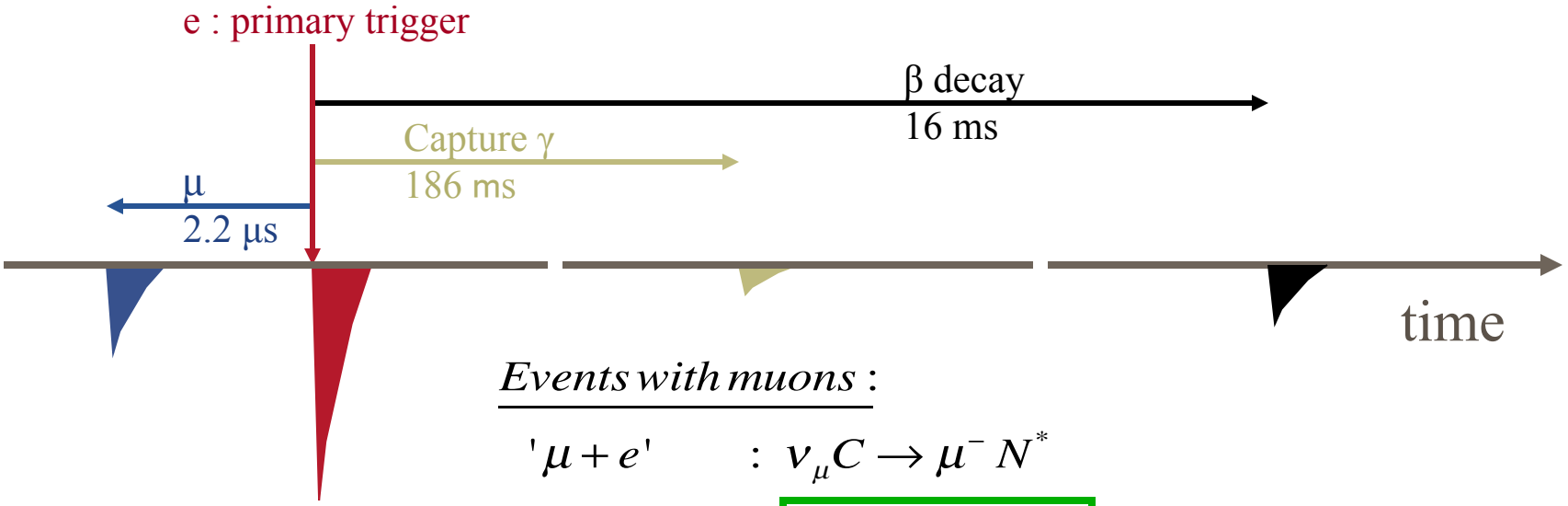

Events with muons :

$$'\mu + e' \quad : \nu_\mu C \rightarrow \mu^- N^*$$

$$'\mu + e + \beta' \quad : \nu_\mu C \rightarrow \mu^- N_{GS}$$

$$'\mu + e + \gamma' \quad : \bar{\nu}_\mu p \rightarrow \mu^+ n$$

Events without muons :

$$'e' \quad : \nu_e e \rightarrow \nu_e e,\ \nu_e C \rightarrow e^- N^* (\nu_\mu \rightarrow \nu_e)$$

$$'e + \beta' \quad : \nu_e C \rightarrow e^- N_{GS}$$

$$'e + \gamma' \quad : \bar{\nu}_e p \rightarrow e^+ n (\bar{\nu}_\mu \rightarrow \bar{\nu}_e)$$

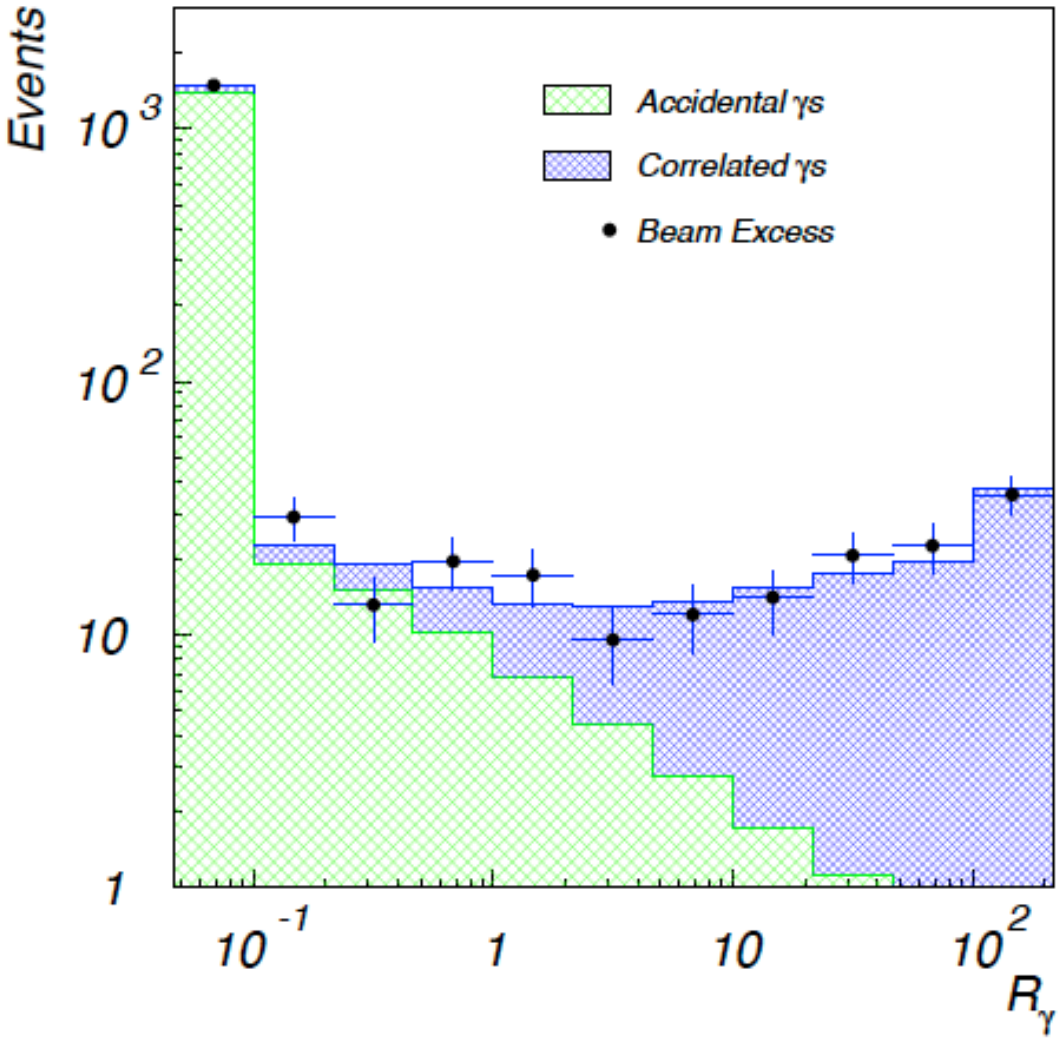

FIG. 12: The R_γ distribution for $\nu_\mu C \to \mu^- N$, $\bar{\nu}_\mu C \to \mu^+ B$, and $\bar{\nu}_\mu p \to \mu^+ n$ inclusive scattering events.

Event Time Structure

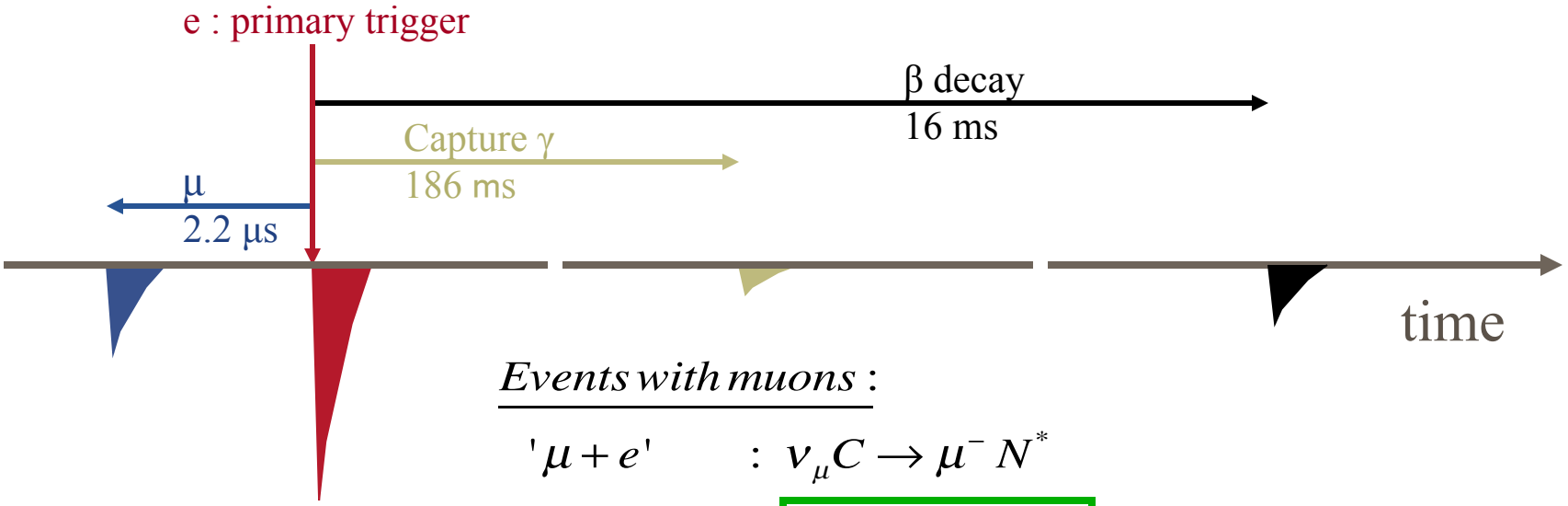

Events with muons :

$$'\mu + e' \quad : \nu_\mu C \rightarrow \mu^- N^*$$

$$'\mu + e + \beta' \quad : \nu_\mu C \rightarrow \mu^- N_{GS}$$

$$'\mu + e + \gamma' \quad : \bar{\nu}_\mu p \rightarrow \mu^+ n$$

Events without muons :

$$'e' \quad : \nu_e e \rightarrow \nu_e e,\ \nu_e C \rightarrow e^- N^* (\nu_\mu \rightarrow \nu_e)$$

$$'e + \beta' \quad : \nu_e C \rightarrow e^- N_{GS}$$

$$'e + \gamma' \quad : \bar{\nu}_e p \rightarrow e^+ n (\bar{\nu}_\mu \rightarrow \bar{\nu}_e)$$

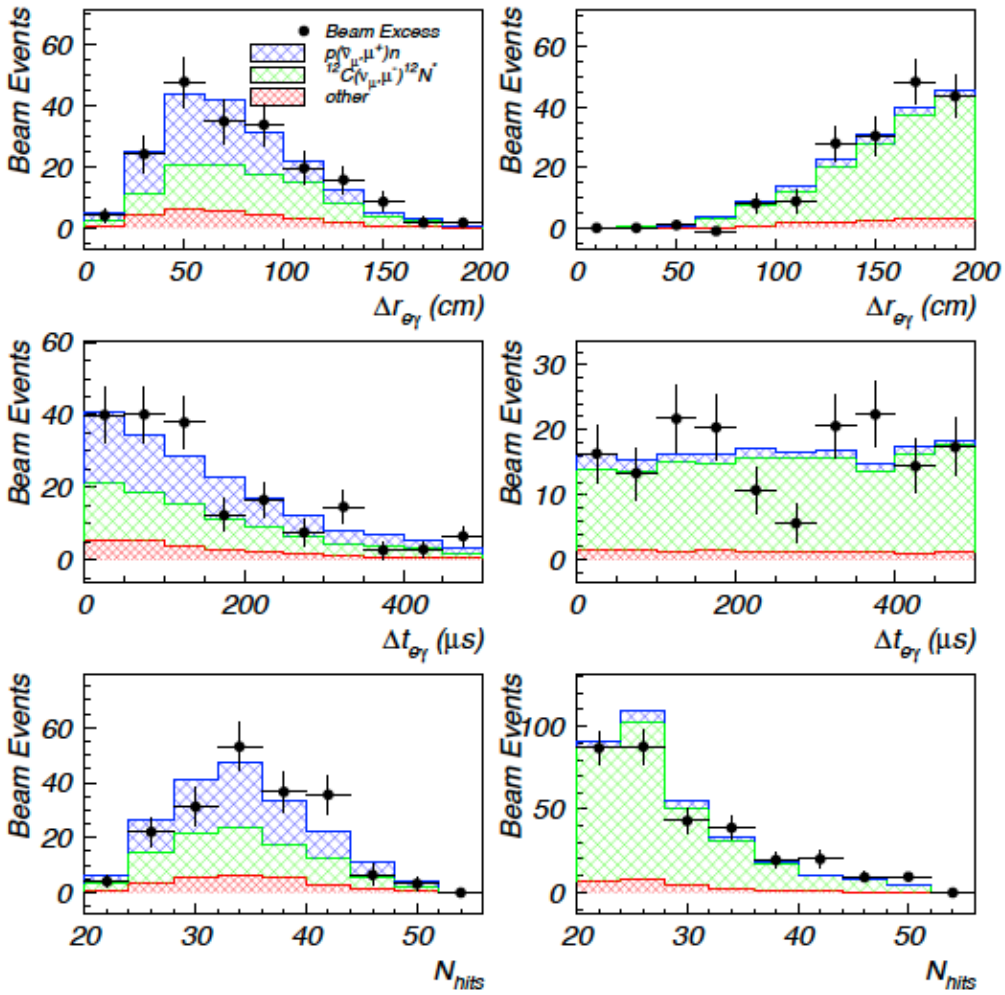

FIG. 13: The individual γ distributions from $\nu_\mu C \to \mu^- N$, $\bar{\nu}_\mu C \to \mu^+ B$, and $\bar{\nu}_\mu p \to \mu^+ n$ scattering for events with $R_\gamma > 1$ (left side) and $R_\gamma < 1$ (right side). The top plots show the distance between the reconstructed γ position and positron position, Δr, the middle plots show the time interval between the γ and positron, Δt, and the bottom plots show the number of hit phototubes associated with the γ, N_{hits}.

Event Time Structure

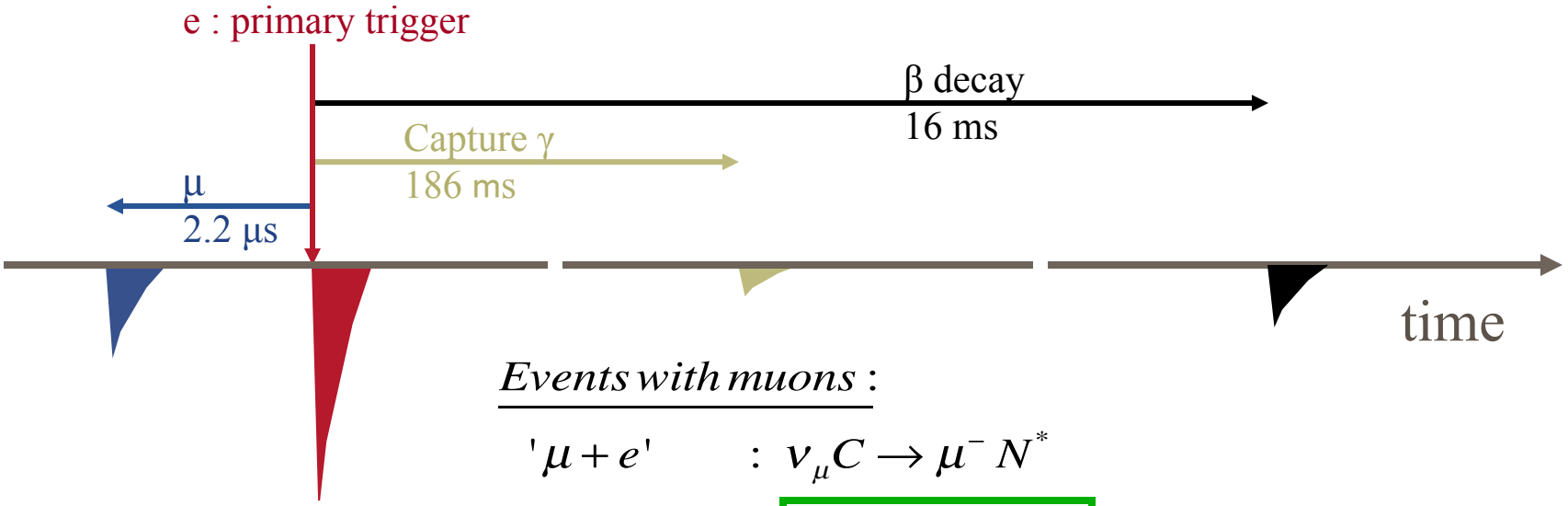

Events with muons :

$$'\mu + e' \quad : \nu_\mu C \rightarrow \mu^- N^*$$

$$'\mu + e + \beta' \quad : \nu_\mu C \rightarrow \mu^- N_{GS}$$

$$'\mu + e + \gamma' \quad : \bar{\nu}_\mu p \rightarrow \mu^+ n$$

Events without muons :

$$'e' \quad : \nu_e e \rightarrow \nu_e e,\ \nu_e C \rightarrow e^- N^* (\nu_\mu \rightarrow \nu_e)$$

$$'e + \beta' \quad : \nu_e C \rightarrow e^- N_{GS}$$

$$'e + \gamma' \quad : \bar{\nu}_e p \rightarrow e^+ n (\bar{\nu}_\mu \rightarrow \bar{\nu}_e)$$

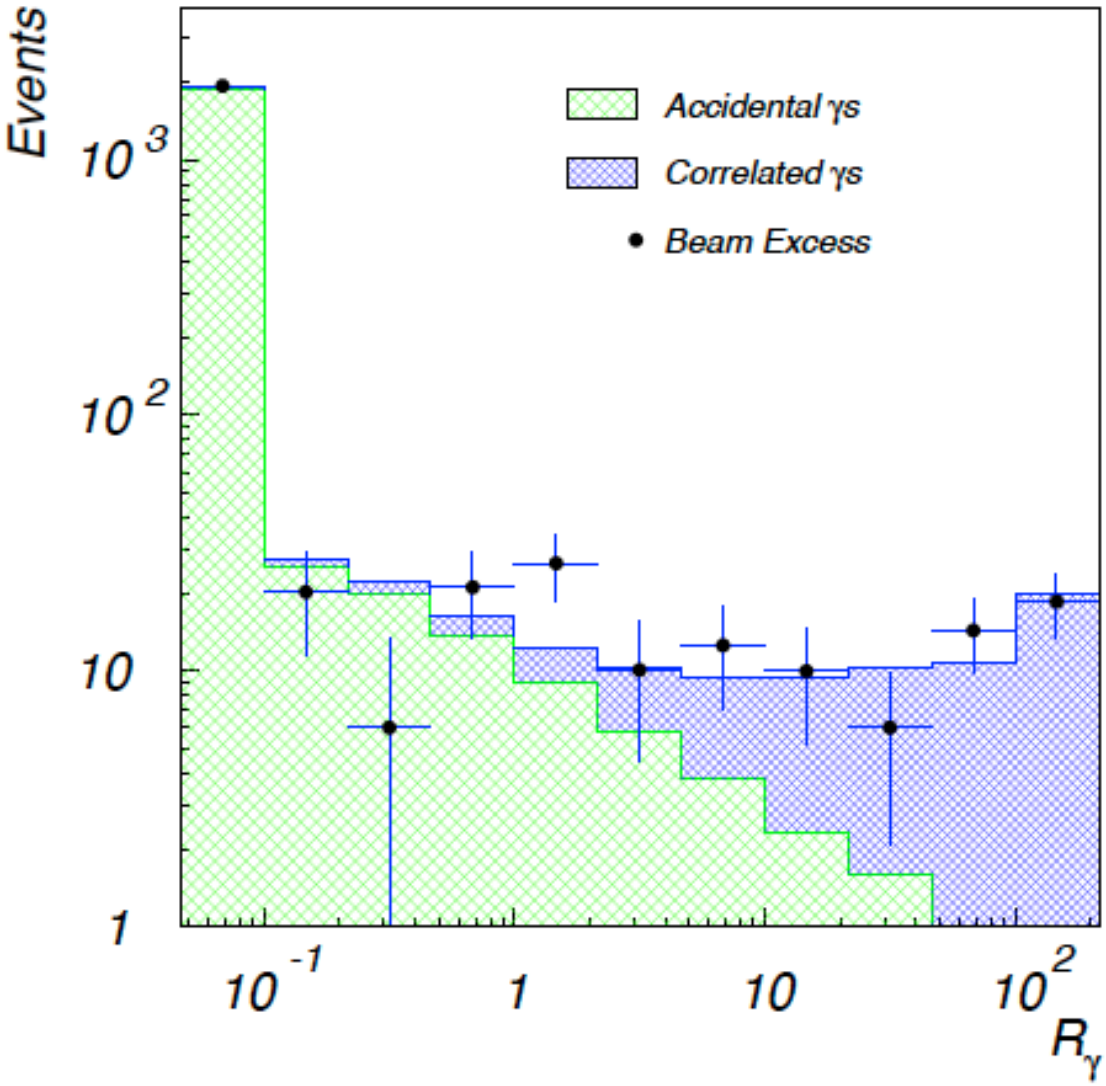

FIG. 14: The R_γ distribution for events that satisfy the selection criteria for the primary $\bar{\nu}_\mu \to \bar{\nu}_e$ oscillation search.

Event Time Structure

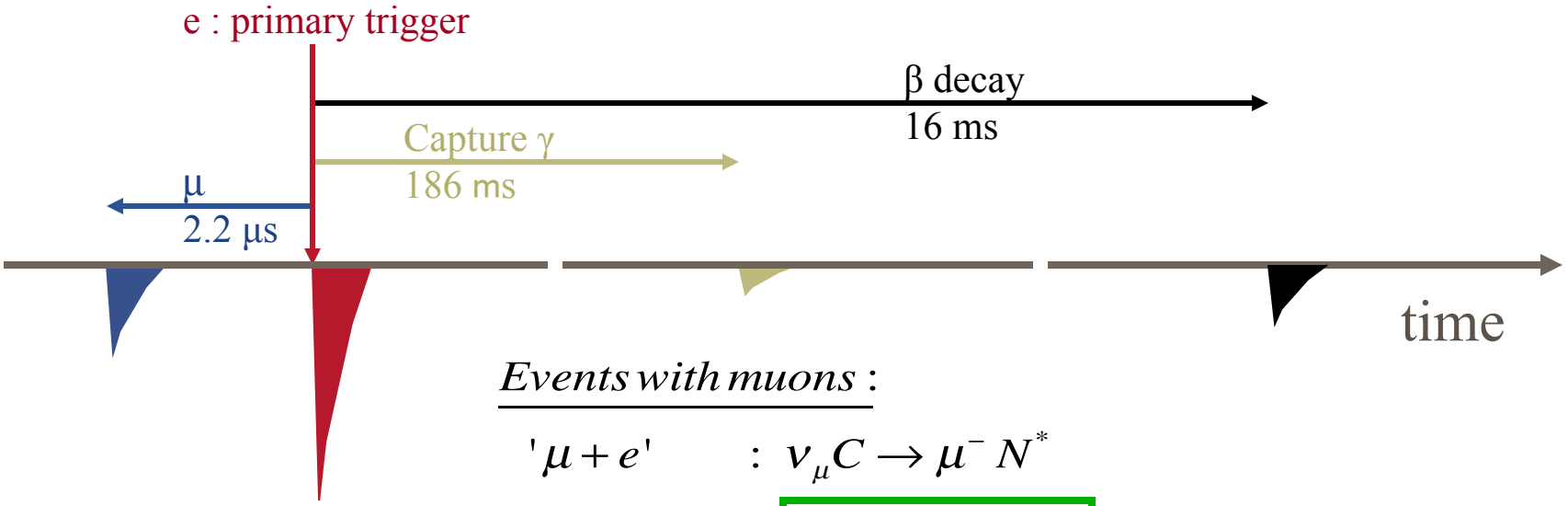

Events with muons :

$$'\mu + e' \quad : \nu_\mu C \rightarrow \mu^- N^*$$

$$'\mu + e + \beta' \quad : \nu_\mu C \rightarrow \mu^- N_{GS}$$

$$'\mu + e + \gamma' \quad : \bar{\nu}_\mu p \rightarrow \mu^+ n$$

Events without muons :

$$'e' \quad : \nu_e e \rightarrow \nu_e e,\ \nu_e C \rightarrow e^- N^* (\nu_\mu \rightarrow \nu_e)$$

$$'e + \beta' \quad : \nu_e C \rightarrow e^- N_{GS}$$

$$'e + \gamma' \quad : \bar{\nu}_e p \rightarrow e^+ n (\bar{\nu}_\mu \rightarrow \bar{\nu}_e)$$

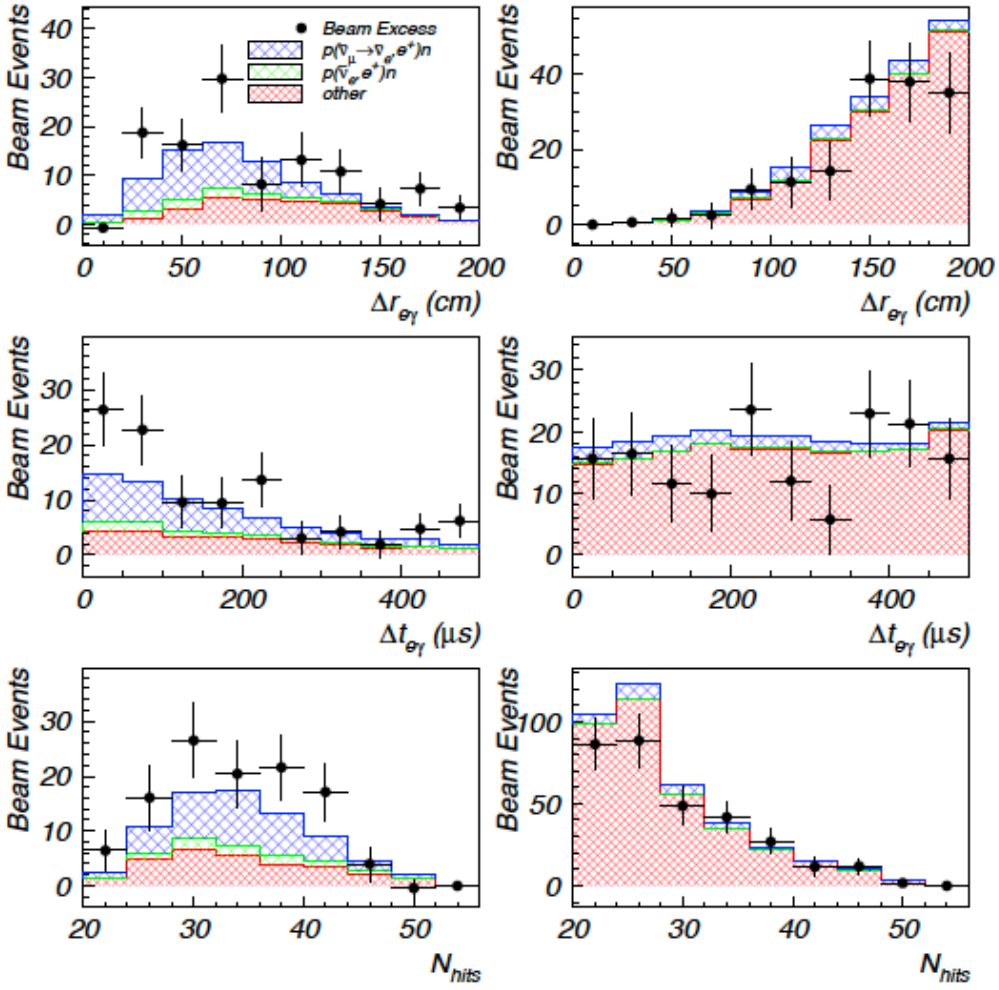

FIG. 15: The individual γ distributions for events that satisfy the selection criteria for the primary $\bar{\nu}_\mu \to \bar{\nu}_e$ oscillation search with $R_\gamma > 1$ (left side) and $R_\gamma < 1$ (right side). The top plots show the distance between the reconstructed γ position and positron position, Δr, the middle plots show the time interval between the γ and positron, Δt, and the bottom plots show the number of hit phototubes associated with the γ, N_{hits}.

Event Time Structure

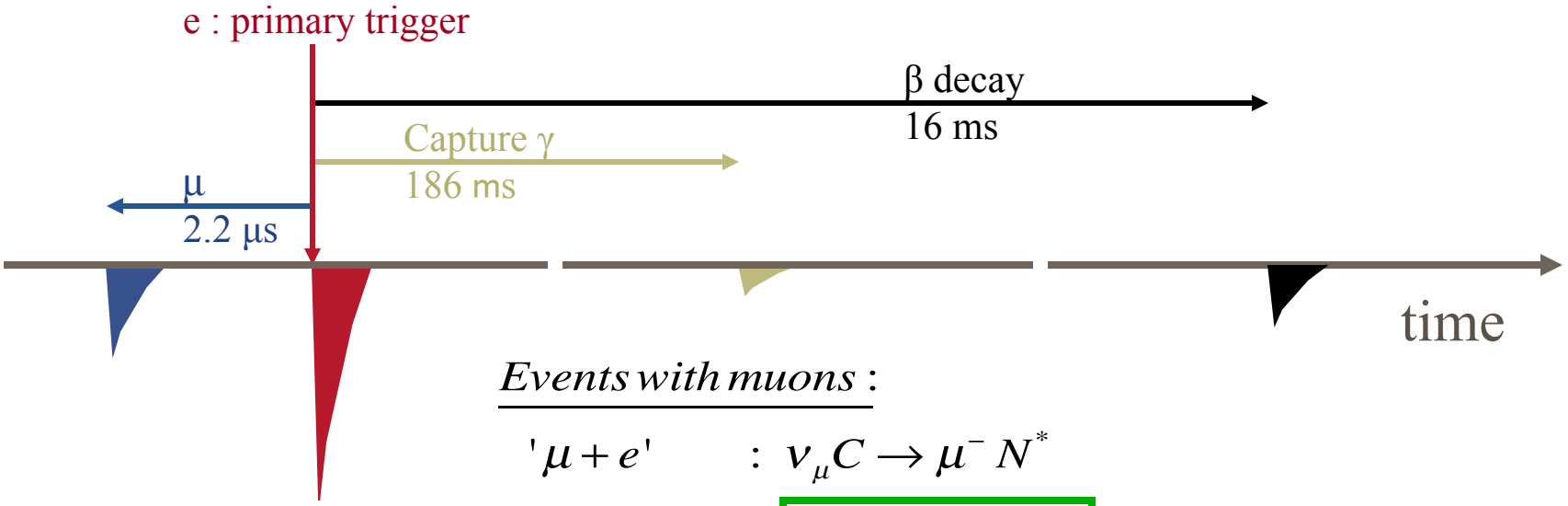

Events with muons :

$$'\mu + e' \quad : \nu_\mu C \rightarrow \mu^- N^*$$

$$'\mu + e + \beta' \quad : \nu_\mu C \rightarrow \mu^- N_{GS}$$

$$'\mu + e + \gamma' \quad : \bar{\nu}_\mu p \rightarrow \mu^+ n$$

Events without muons :

$$'e' \quad : \nu_e e \rightarrow \nu_e e,\ \nu_e C \rightarrow e^- N^* (\nu_\mu \rightarrow \nu_e)$$

$$'e + \beta' \quad : \nu_e C \rightarrow e^- N_{GS}$$

$$'e + \gamma' \quad : \bar{\nu}_e p \rightarrow e^+ n (\bar{\nu}_\mu \rightarrow \bar{\nu}_e)$$

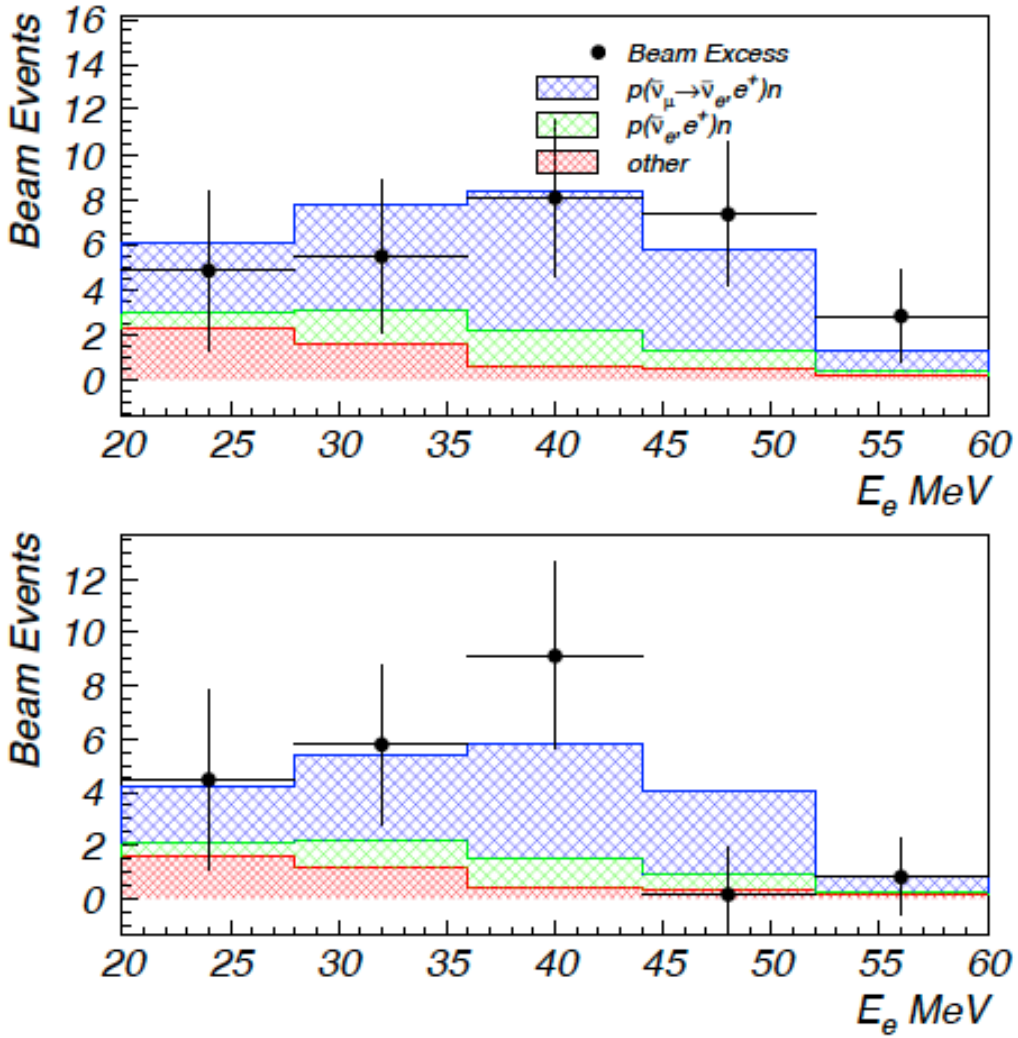

FIG. 17: The energy distribution of the 1993-1995 (top plot) and 1996-1998 (bottom plot) data samples for events with $R_\gamma > 10$. The shaded region shows the expected distribution from a combination of neutrino background plus neutrino oscillations at low Δm^2.

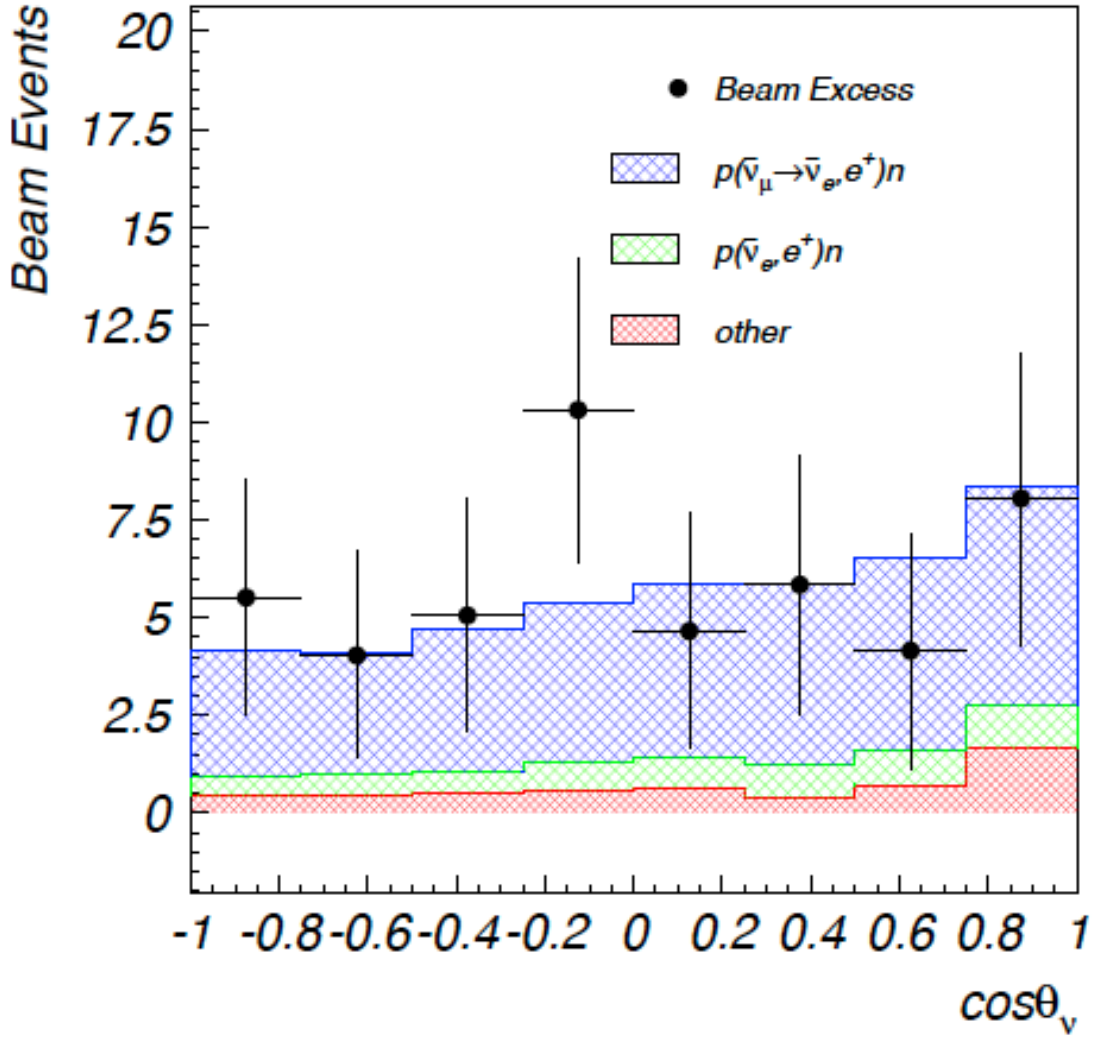

FIG. 18: The $\cos\theta_\nu$ distribution for events with $R_\gamma > 1$ and $36 < E < 60$ MeV. The shaded region shows the expected distribution from a combination of neutrino background plus neutrino oscillations at low Δm^2.

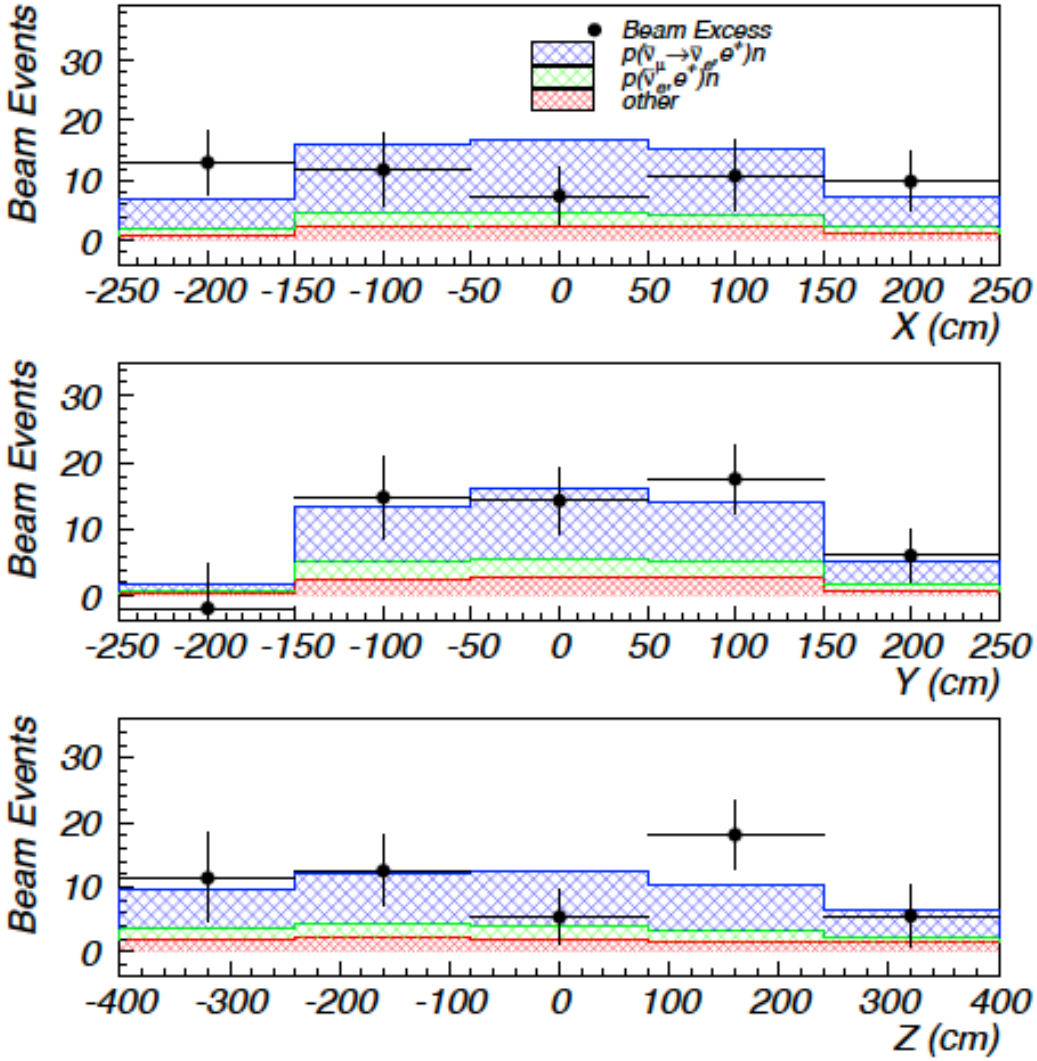

FIG. 19: The spatial distributions for events with $R_\gamma > 10$, $20 < E_e < 60$ MeV, and $D > 10$ cm. The shaded region shows the expected distribution from a combination of neutrino background plus neutrino oscillations at low Δm^2.

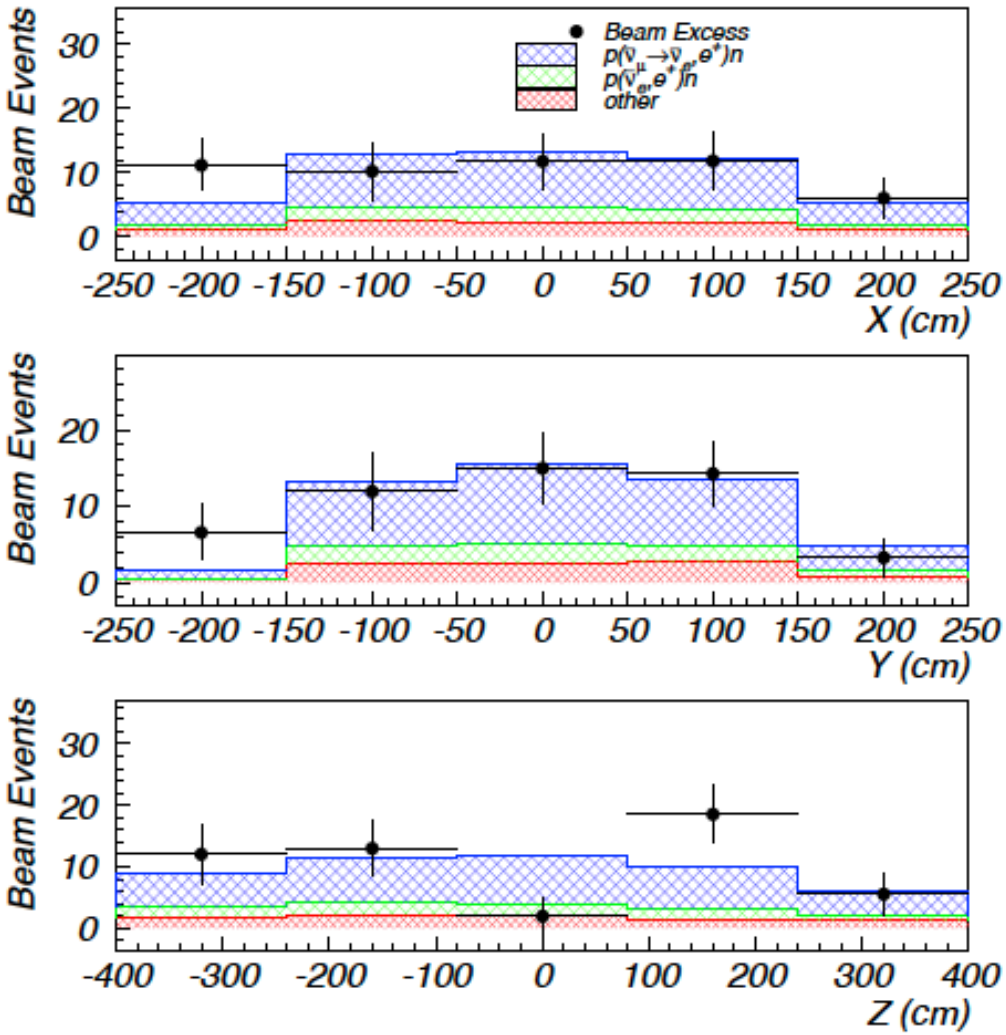

FIG. 20: The spatial distributions for events with $R_\gamma > 10$, $20 < E_e < 60$ MeV, and $D > 35$ cm. The shaded region shows the expected distribution from a combination of neutrino background plus neutrino oscillations at low Δm^2.

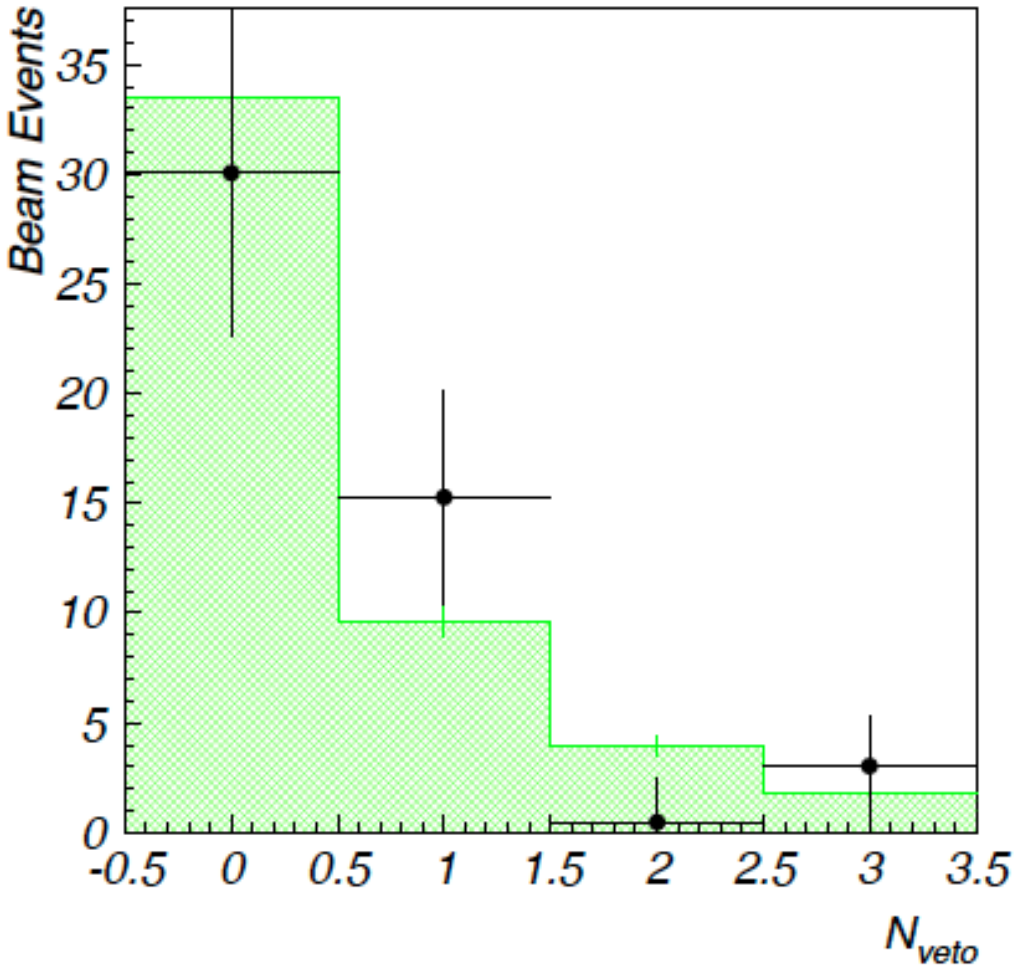

FIG. 23: The veto hit distribution for events with $R_\gamma > 10$ and $20 < E_e < 60$ MeV. The data agree well with the distribution from $\nu_e C \rightarrow e^- N_{g.s.}$ scattering (shaded histogram), where the reaction is identified by the $N_{g.s.}$ β decay.

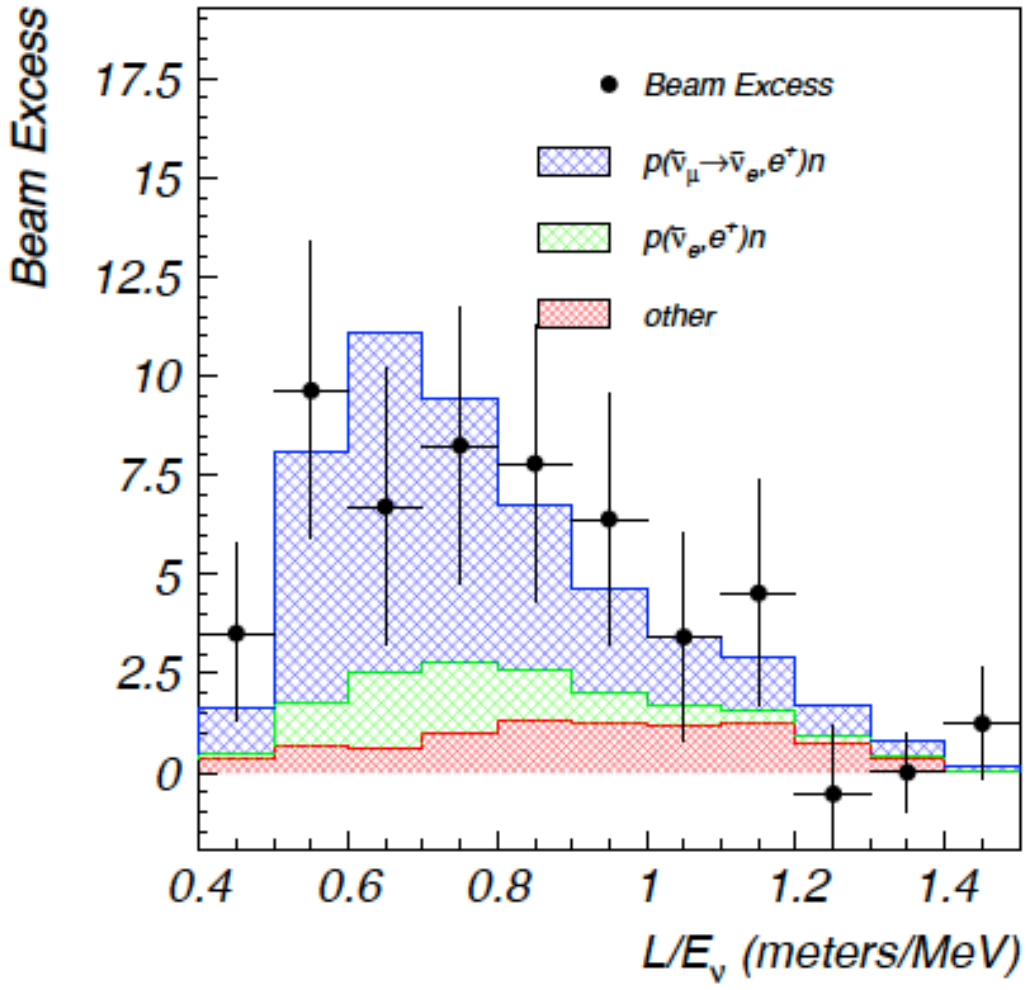

FIG. 24: The L_ν/E_ν distribution for events with $R_\gamma > 10$ and $20 < E_e < 60$ MeV, where L_ν is the distance travelled by the neutrino in meters and E_ν is the neutrino energy in MeV. The data agree well with the expectation from neutrino background and neutrino oscillations at low Δm^2.

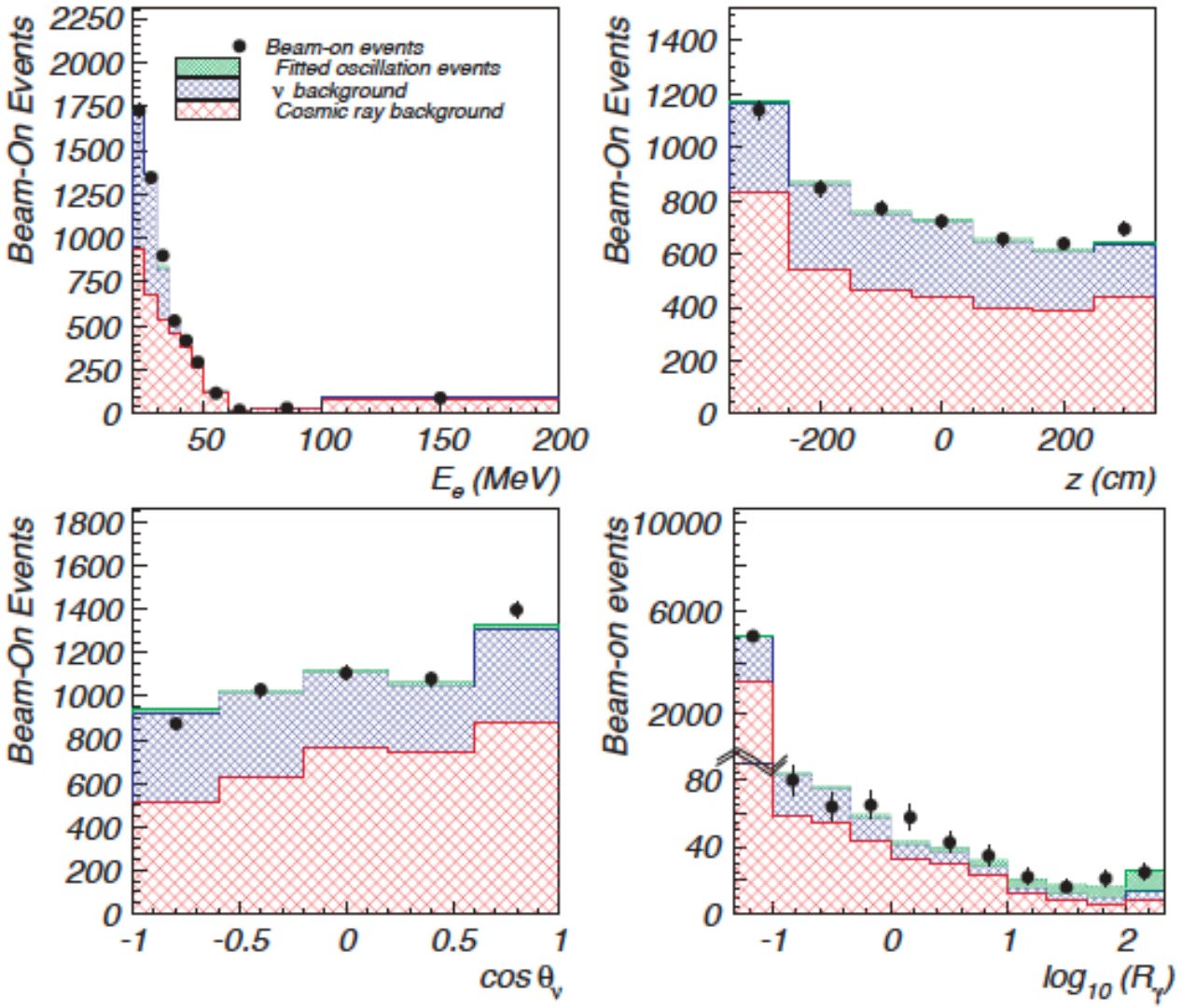

FIG. 28: The E_e, z, $\cos\theta_\nu$, and R_γ projections from the 4-dimensional $(\sin^2 2\theta, \Delta m^2)$ likelihood fit. The points with error bars are the data.

TABLE VIII: The estimated number of events in the $20 < E_e < 60$ MeV energy range due to 100% $\bar{\nu}_\mu \rightarrow \bar{\nu}_e$ transmutation and to the two beam-related backgrounds with neutrons, μ^- decay at rest in the beam stop followed by $\bar{\nu}_e p \rightarrow e^+ n$ scattering in the detector and π^- decay in flight in the beam stop followed by $\bar{\nu}_\mu p \rightarrow \mu^+ n$ scattering. The π^- DIF background includes contributions from $\bar{\nu}_\mu C \rightarrow \mu^+ n X$ and $\nu_\mu C \rightarrow \mu^- n X$ scattering, as well as a small $\bar{\nu}_e$ background from π^- and μ^- DIF. The events must satisfy the electron selection criteria, but no correlated γ requirement is imposed.

Neutrino Source	Reaction	Number of Events
μ^+ DAR	100% $\bar{\nu}_\mu \rightarrow \bar{\nu}_e$	33300 ± 3300
μ^- DAR	$\bar{\nu}_e p \rightarrow e^+ n$	19.5 ± 3.9
π^- DIF	$\bar{\nu}_\mu p \rightarrow \mu^+ n$	10.5 ± 4.6

TABLE IX: The correlated and accidental γ efficiencies for different R_γ selections. The systematic uncertainty of these efficiencies is estimated to be $\pm 7\%$ of their values.

Selection	Correlated γ Efficiency	Accidental γ Efficiency
$R_\gamma > 1$	0.51	0.012
$R_\gamma > 10$	0.39	0.0026
$R_\gamma > 100$	0.17	0.0002

TABLE X: Numbers of beam-on events that satisfy the selection criteria for the primary $\bar{\nu}_\mu \to \bar{\nu}_e$ oscillation search with $R_\gamma > 1$, $R_\gamma > 10$, and $R_\gamma > 100$. Also shown are the beam-off background, the estimated neutrino background, the excess of events that is consistent with neutrino oscillations, and the probability that the excess is due to a statistical fluctuation.

Selection	Beam-On Events	Beam-Off Background	ν Background	Event Excess	Probability
$R_\gamma > 1$	205	106.8 ± 2.5	39.2 ± 3.1	$59.0 \pm 14.5 \pm 3.1$	7.8×10^{-6}
$R_\gamma > 10$	86	36.9 ± 1.5	16.9 ± 2.3	$32.2 \pm 9.4 \pm 2.3$	1.1×10^{-4}
$R_\gamma > 100$	27	8.3 ± 0.7	5.4 ± 1.0	$13.3 \pm 5.2 \pm 1.0$	1.8×10^{-3}

TABLE XI: The number of excess events in the $20 < E_e < 60$ MeV energy range, together with the corresponding oscillation probability if the excess is due to $\bar{\nu}_\mu \to \bar{\nu}_e$ oscillations. Also shown are the results from the analysis of the 1993-1995 data sample [2].

Analysis	Excess Events	Oscillation Probability
Present Analysis (1993-1998)	$87.9 \pm 22.4 \pm 6.0$	$(0.264 \pm 0.067 \pm 0.045)\%$
Previous Analysis (1993-1995)	$51.0^{+20.2}_{-19.5} \pm 8.0$	$(0.31 \pm 0.12 \pm 0.05)\%$

TABLE XIII: Number of beam on-off excess events that satisfy the selection criteria for the primary $\bar{\nu}_\mu \to \bar{\nu}_e$ oscillation search with 1 associated γ and with > 1 associated γ. (An associated γ is defined to have $R_\gamma > 10$.) The excess of events with > 1 correlated γ is approximately zero, which is what is expected for the reaction $\bar{\nu}_e p \to e^+ n$.

Energy Selection	1 Associated γ	> 1 Associated γ
$20 < E_e < 60$ MeV	49.1 ± 9.4	-2.8 ± 2.4
$36 < E_e < 60$ MeV	28.3 ± 6.6	-3.0 ± 1.7

TABLE XIV: Number of beam on-off excess events that satisfy the selection criteria for the primary $\bar{\nu}_\mu \rightarrow \bar{\nu}_e$ oscillation search with $36 < E_e < 60$ MeV and with > 11 "lookback" hits in the 0-3 μs and 3-6 μs intervals. Results are shown for events with $R_\gamma \geq 0$ and for events with $R_\gamma > 10$. The number of excess events in each 3μs interval is consistent with the probability of having an accidental lookback in the time interval.

R_γ Selection	$0-3\mu$s	$3-6\mu$s	Events Expected Due to Accidentals
$R_\gamma \geq 0$	11.5 ± 6.3	7.8 ± 5.9	10.8 ± 2.2
$R_\gamma > 10$	1.7 ± 1.4	0.5 ± 1.0	1.6 ± 0.4

TABLE XV: The number of excess events in the $60 < E_e < 200$ MeV energy range, together with the corresponding oscillation probability if the excess is due to $\nu_\mu \rightarrow \nu_e$ oscillations. Also shown are the results from the higher precision analysis of the 1993-1995 data sample [3].

Analysis	Excess Events	Oscillation Probability
Present Analysis (1993-1998)	$8.1 \pm 12.2 \pm 1.7$	$(0.10 \pm 0.16 \pm 0.04)\%$
Previous Analysis (1993-1995)	$18.1 \pm 6.6 \pm 4.0$	$(0.26 \pm 0.10 \pm 0.05)\%$

TABLE XVI: The eight contributions to the $(\sin^2 2\theta, \Delta m^2)$ $\mathcal{L}$ fit from all of the signal and background processes. Also shown are the fitted number of events at the best fit point of $(\sin^2 2\theta, \Delta m^2)_{best-fit} = (0.003, 1.2\text{eV}^2)$.

$\mathcal{L}$ Contribution	Signal or Background Source	Process	Fitted Number of Events
1	$\overline{\nu}_\mu \to \overline{\nu}_e$	$\bar{\nu}_e p \to e + n$	89.5
2	BUB		3664.6
3	DAR ν_e	$\nu_e\ ^{12}C \to e^- N_{g.s.}$	1865.0
		$\nu_e\ ^{12}C \to e^- N^*$	
		$\nu_e\ ^{13}C \to e^- N$	
		$\nu e \to \nu e$	
4	DIF ν_μ	$\nu_\mu C \to \mu^- N^*$	37.3
		$\nu_\mu C \to \mu^- N_{g.s.}$	
5	DIF $\overline{\nu}_\mu$	$\overline{\nu}_\mu p \to \mu^+ n$	5.9
		$\overline{\nu}_\mu C \to \mu^+ B^*$	
		$\overline{\nu}_\mu C \to \mu^+ B_{g.s.}$	
6	DAR $\overline{\nu}_e$ (μ^- DAR)	$\overline{\nu}_e p \to e^+ n$	16.7
7	$\nu_\mu \to \nu_e$	$\nu_e C \to e^- N$	6.1
8	DIF $\pi^+ \to \nu_e$ and $\mu^+ \to \nu_e$ decay	$\nu_e C \to e^- N$	11.9

TABLE XVII: A comparison of the LSND and KARMEN experiments.

Property	LSND	KARMEN
Proton Energy	798 MeV	800 MeV
Proton Intensity	1000 μA	200 μA
Duty Factor	6×10^{-2}	1×10^{-5}
Total Mass	167 t	56 t
Neutrino Distance	30 m	17.5 m
Particle Identification	YES	NO
Energy Resolution at 50 MeV	6.6%	1.6%

LSND Neutrino Physics, G B Mills